Petrogenesis and tectonic evolution of metaluminous sub-alkaline granitoids from the Takab Complex, NW Iran

ROBAB HAJIALIOGHLI*§, MOHSSEN MOAZZEN*, AHMAD JAHANGIRI*,
ROLAND OBERHÄNSLI†, BEATE MOCEK‡¶ & UWE ALTENBERGER†

*Department of Geology, University of Tabriz, 51664, Tabriz, Iran
†Institut für Geowissenschaften, Universität Potsdam, Germany
‡Department of Geology, University of Kansas, Lawrence, Kansas, USA

Abstract – The Takab complex is composed of a variety of metamorphic rocks including amphibolites, metapelites, mafic granulites, migmatites and meta-ultramafics, which are intruded by the granitoid. The granitoid magmatic activity occurred in relation to the subduction of the Neo-Tethys oceanic crust beneath the Iranian crust during Tertiary times. The granitoids are mainly granodiorite, quartz monzodiorite, monzonite and quartz diorite. Chemically, the magmatic rocks are characterized by ASI < 1.04, AI < 0.87 and high contents of CaO (up to ∼ 14.5 wt %), which are consistent with the I-type magmatic series. Low $FeO_t/(FeO_t+MgO)$ values (< 0.75) as well as low Nb, Y and K_2O contents of the investigated rocks resemble the calc-alkaline series. Low SiO_2, K_2O/Na_2O and Al_2O_3 accompanied by high CaO and FeO contents indicate melting of metabasites as an appropriate source for the intrusions. Negative Ti and Nb anomalies verify a metaluminous crustal origin for the protoliths of the investigated igneous rocks. These are comparable with compositions of the associated mafic migmatites, in the Takab metamorphic complex, which originated from the partial melting of amphibolites. Therefore, crustal melting and a collision-related origin for the Takab calc-alkaline intrusions are proposed here on the basis of mineralogy and geochemical characteristics. The *P–T* evolution during magmatic crystallization and subsolidus cooling stages is determined by the study of mineral chemistry of the granodiorite and the quartz diorite. Magmatic crystallization pressure and temperature for the quartz-diorite and the granodiorite are estimated to be $P \sim 7.8 \pm 2.5$ kbar, $T \sim 760 \pm 75\,°C$ and $P \sim 5 \pm 1$ kbar, $T \sim 700\,°C$, respectively. Subsolidus conditions are consistent with temperatures of ∼ 620 °C and ∼ 600 °C, and pressures of ∼ 5 kbar and ∼ 3.5 kbar for the quartz-diorite and the granodiorite, respectively.

Keywords: granitoids, partial melting, Neo-Tethys, Takab, NW Iran.

In Memory of Doctor Beate Mocek (1962–2010)

1. Introduction

The Takab complex of northwest Iran is located within the Alpine–Himalayan orogenic system. The Takab complex has been assigned to various tectonic subdivisions of Iran. It is included in the Central Iran Zone by Berberian & King (1981), at the junction of the Central Iran, the Alborz–Azerbaijan and the Sanandaj–Sirjan zones (Babakhani & Ghalamgash, 1990) and in the Sanandaj–Sirjan Zone (Gilg *et al.* 2006) (Fig. 1a). Geological and lithological characteristics of the Takab area show affinities to the Central Iran micro-continent (Hajialioghli *et al.* 2007*a,b*). Zircon U/Pb dating of granitic gneisses from the Takab area yields an age of 560 Ma (Stockli *et al.* 2004), which is comparable to U/Pb ages of granitic augen gneisses from the Central Iran micro-continent (*c.* 550 Ma: Ramezani & Tucker, 2003) and also similar rock types from the Menderes Massif of Turkey, to the west of the area (520–570 Ma, Loos & Reischmann, 1999). Tertiary magmatism occurred in relation to the subduction of the Neo-

Tethys (Şengör, 1984; Mohajjel & Fergusson, 2000; Mohajjel, Fergusson & Sahandi, 2003). In the context of the timing of closure of the Neo-Tethys and inception of collision between the Arabian and Iranian plates, different opinions are postulated. Berberian & King (1981) and Alavi (1994) advanced a late Cretaceous age for collision along the Zagros suture. Others describe a Cenozoic continental collision (e.g. Eocene: Berberian *et al.* 1982; J. Braud, unpub. Ph.D. thesis, Univ. de Paris-Sud, 1987; Şengör *et al.* 1988; Şengör, Natal'in & Burtman, 1993; Şengör & Natal'in, 1996; Mohajjel, Fergusson & Sahandi, 2003; Ghasemi & Talbot, 2006; Oligocene: Agard *et al.* 2005; and Miocene: Jackson *et al.* 1995; Şengör *et al.* 2008). Based on palinspastic and plate tectonic studies, McQuarrie *et al.* (2003) suggested that the collision between the Iranian plate and the Central Iran micro-continent took place at 20 Ma at the latest, in relation to the subduction of the Neo-Tethys. Recent studies by Verdel *et al.* (2007) support a Neogene collision between the Iranian plate and the Central Iran micro-continent.

The focus of this study is the calc-alkaline granitoids of the Takab area. This is the first study of the petrology, geochemistry and petrogenesis of the Tertiary granitoids in the area. The combination of the data will

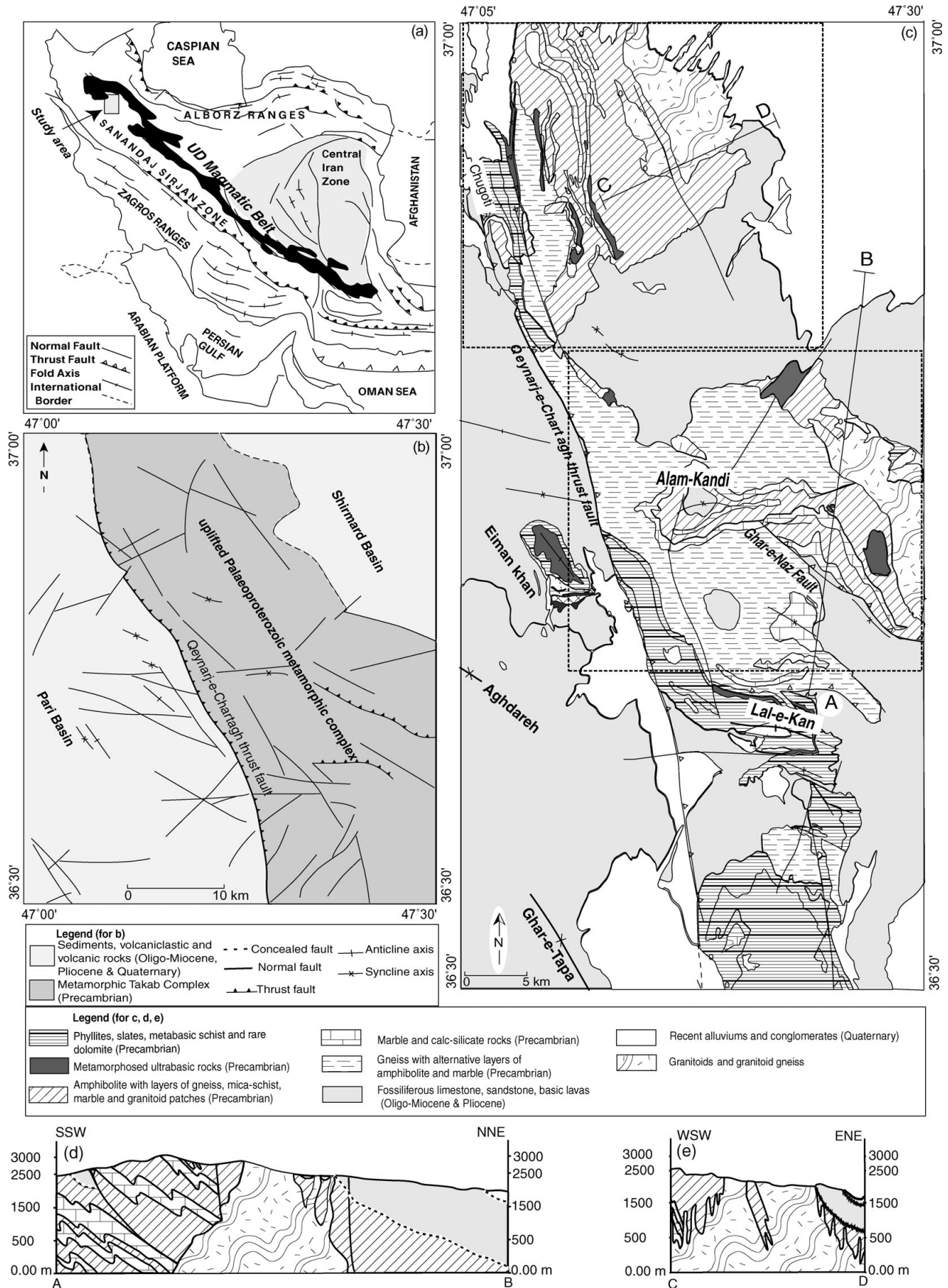§Author for correspondence: hajialioghli@tabrizu.ac.ir
¶Deceased

Figure 1. (a) Structural subdivision map of Iran from Gilg *et al.* (2006). The study area is shown by a rectangle. (b) Structural map of the area. (c) Geological map of the study area, adapted from geological maps of Takht-e-Solyman (Babakhani & Ghalamgash, 1990) with some modifications. Dashed boxes are enlarged in Figure 2. (d, e) Cross-sections across profiles A–B and C–D to show the relations between the rock units in the area.
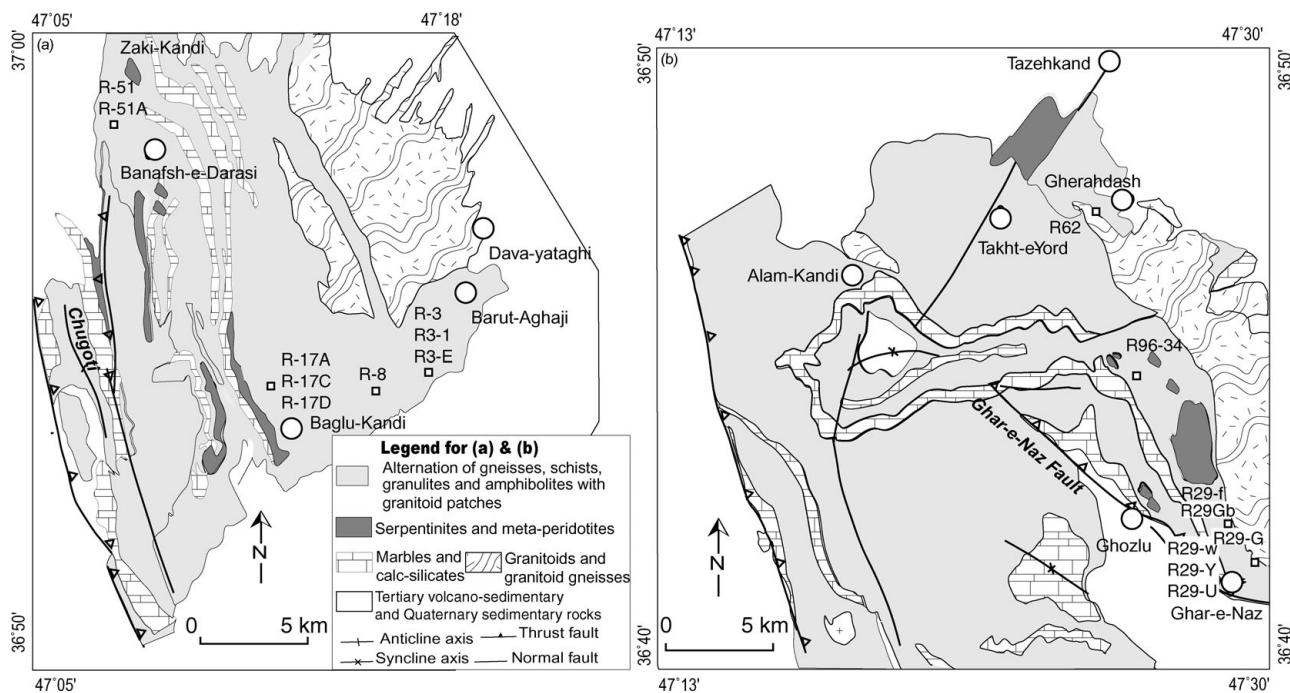
Figure 2. Larger map of the area showing rock units and the sample localities: (a) north of the area and (b) south of the area.

allow us to address the tectonic setting and geochemical significance of these rocks.

The composition of coexisting minerals is used to estimate the *P–T* conditions of equilibration during magmatic crystallization and subsolidus cooling stages of the magmatic rocks.

This study, along with ongoing studies on the associated granulites, amphibolites, metapelites and meta-ultramafic rocks (R. Hajialioghli, unpub. Ph.D. thesis, Univ. Tabriz, 2007; Hajialioghli *et al.* 2007*a*; Moazzen *et al.* 2009), will furnish a framework to decipher the geodynamic history of the Takab and the adjacent areas. This may elucidate the geological history of NW Iran in relation to the Tethyan-related events.

2. Geological setting and field relations

The Takab complex in NW Iran is located between longitude 47°45′ and 47°05′ E and latitude 37°30′ and 36°30′ N. It occurs as a NW–SE-trending horst which is thrust along the reverse faults (Figs 1, 2). The eastern border is marked by the Pari basin. The Qeynarj-e-Chartagh thrust fault forms the western border with the Shirmard basin (Fig. 1b). It consists of a variety of rocks including granulites, metabasites, amphibolites, migmatites, calc-silicate rocks, meta-ultramafics, gneisses, mica-schists and sporadically, granitoids (Hajialioghli *et al.* 2007*a,b*; Moazzen *et al.* 2009; Saki, 2010). The oldest crustal protolith of the Takab basement has been dated about 2961 ± 72 Ma ($^{206}Pb/^{238}U$–$^{207}Pb/^{235}U$) and 2775–2875 Ma (^{204}Pb corrected $^{207}Pb/^{206}Pb$) (R. Hajialioghli, unpub. Ph.D. thesis, Univ, Tabriz, 2007; Moazzen & Hajialioghli, 2008), comparatively similar to the ages from the

Central Iran micro-continent (*c.* 2140 Ma, $^{207}Pb/^{206}Pb$: Ramezani & Tucker, 2003 and *c.* 2382 Ma, Rb/Sr whole rock ages: Haghipour, 1974) and Bozburun of southeastern Turkey, to the west of the study area (*c.* 2522 Ma, $^{207}Pb/^{206}Pb$: Kröner & Şengör, 1990).

The Takab complex experienced regional metamorphism in Precambrian times, overprinted by another high-grade metamorphism during Tertiary times, producing the migmatites and the granitoids (very similar to Central Iran: Ramezani & Tucker, 2003). The age for Precambrian metamorphism is documented by dating on gneisses of the area by Stockli *et al.* (2004), and the age for migmatization and resulted granitoids is indicated by zircon SHRIMP dating (R. Hajialioghli, unpub. Ph.D. thesis, Univ. Tabriz, 2007; Moazzen & Hajialioghli, 2008).

Migmatization of the crustal rocks in the Takab area occurred at *c.* 25 Ma (U/Pb dating on zircons from the leucosome parts of the migmatites: R. Hajialioghli, unpub. Ph.D. thesis, Univ. Tabriz, 2007; Moazzen & Hajialioghli, 2008), corresponding to the Alpine orogeny. The granitoids studied here are small and scattered exposures within the metamorphic rocks. They appear as voluminous leucosome parts of migmatites in places and also as isolated granitic bodies within the metamorphic rocks (Fig. 3), indicating possible short-distance migration of the leucosome parts, coalescence of the melt and formation of the granitoid patches. The sizes of these granitic patches are too small to be shown on the map. Only the sampling locations are shown. The old metamorphic rocks and the granitoids are unconformably overlain by the Oligo-Miocene volcanic and sedimentary rocks (Fig. 1c–e). The Oligo-Miocene sedimentary rocks include basal conglomerate, marl and red sandstone. The
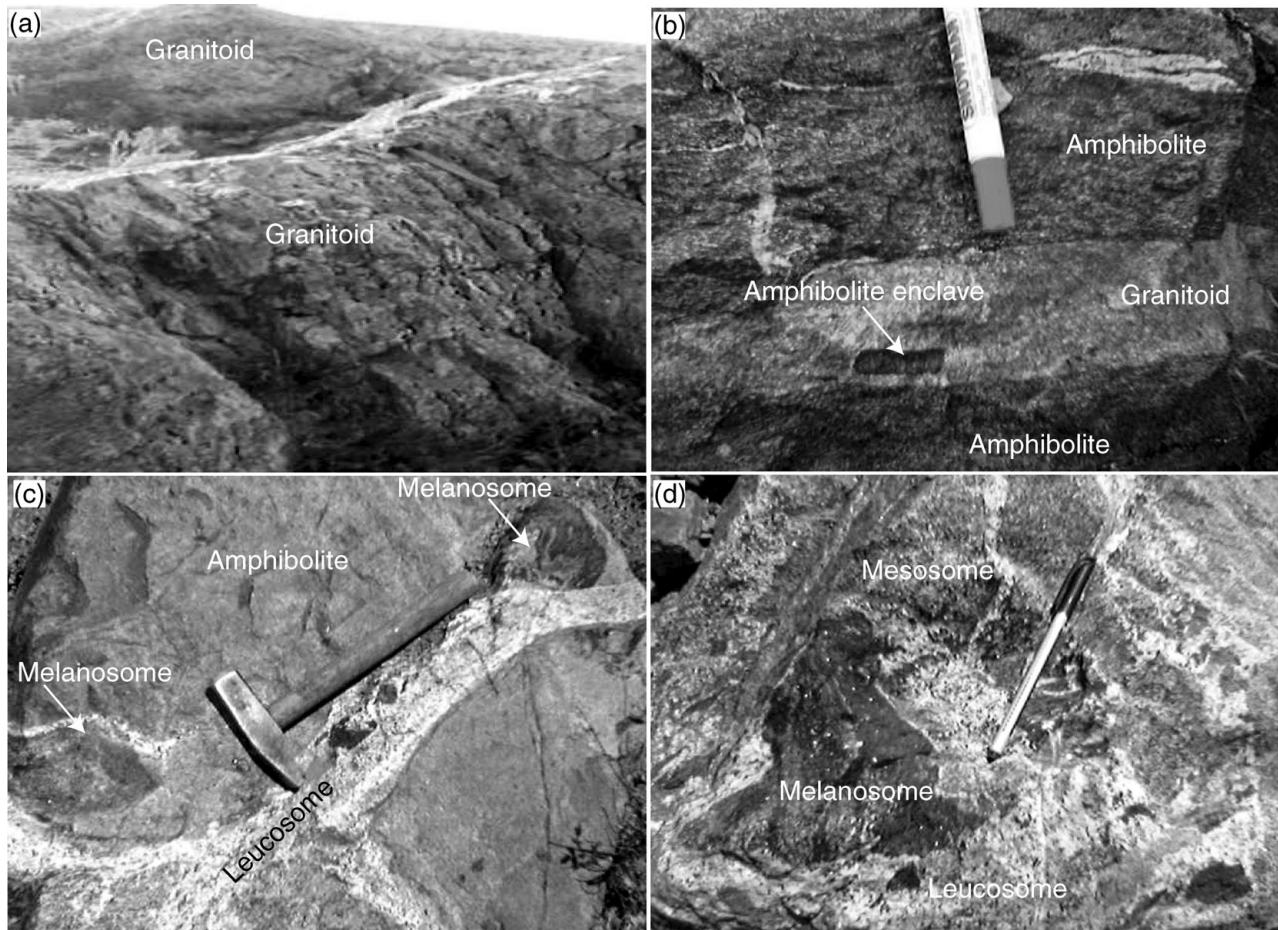
Figure 3. Field photographs of the granitoids and the migmatitic rocks. (a) Limited outcrop of granitoids. The width of the photo is ∼ 2 m. (b) Granitoid patches intruded the amphibolites with small amphibolite enclave. Visible portion of marker is 11 cm long. (c) Leucosome portion of migmatite cross-cutting the rocks. Length of hammer is 33 cm. (d) Mesosome and melanosome parts 'floating' in the granitoid leucosome. Length of pen is 16 cm.

conglomerate is polygenetic, having various fragments of metamorphic rocks (Babakhani & Ghalamgash, 1990). Alluviums and enormous deposits of travertine along the thrust faults are Quaternary in age (Figs 1, 2).

Considering the lack of Palaeozoic and Mesozoic sediments, Babakhani & Ghalamgash (1990) believed that the Takab metamorphic basement most probably was a high region during Palaeozoic and Mesozoic times.

There is no published account on the radiometric age of the granitoids, but as discussed below, a Tertiary age can be considered for them. On the basis of field relations, Lotfi (2001) considered the relative age of the granitoids to be post-Cretaceous. Mazhari *et al.* (2009) believed these granitoids to be Tertiary, and Babakhani & Ghalamgash (1990) also considered the granitoids to be Tertiary in age. The late Palaeozoic and Mesozoic rocks are lacking in this area. In addition, Oligo-Miocene sediments and volcanic rocks unconformably cover the metamorphic basement rocks and the granitoids. Fragments of amphibolites and gneisses appear as enclaves in granodiorite in some places. There are sharp contacts between amphibolite and granodiorite in the SW Barut-Aghaji and north of

the village of Baglu-kandi (Figs 1, 3b). Mineralogically the Takab granitoids are very similar to plutonic rocks from the Sanandaj–Sirjan Zone of the Zagros belt and the Central Iran Zone (e.g. Mazhari *et al.* 2009), which are mainly Tertiary in age and are related to the Neo-Tethys oceanic crust subduction and the subsequent collision. U/Pb zircon dating on migmatites, which are spatially associated with granitoid intrusions, gives an age of *c.* 25 Ma (R. Hajialioghli, unpub. Ph.D. thesis, Univ. Tabriz, 2007). Taking all these facts together, a Tertiary age for the studied granitoids is very likely. However, appropriate age dating studies will furnish more information in this regard.

Faulting and folding of the Oligo-Miocene sediments and volcanic rocks (Aghdareh anticline in the SW of the study area, which consists of Oligo-Miocene limestone, marl and andesite and Ghar-e-Tapa anticline in the SW having folded Oligo-Miocene conglomerate and sandstone; Fig. 1), refolding of the Precambrian metamorphic complex (Lal-e-Kan anticline in south and Chughoti anticline in the NW of the area; Fig. 1) and occurrence of Miocene–Pliocene continental sediments related to the collisional regime, are results of Alpine orogeny in the area. All rock units in the area show a NW–SE trend, parallel to the main

Table 1. Mineral composition (modal %) of the granitoids and migmatitic leucosomes from the Takab area

Rock type	Granite	Granodiorite	Qtz-monzodiorite	Qtz-diorite	Migmatitic leucosome
Rock sample	R29-U, R-3, R-51, R3-E	R3–1, R17-d, R8-K, R-51A	R29-F, R8-J, R17-C	R29-W, R29-Y, R17-A, R29-G	R29–1
K-feldspar	10–20	7–15	7–10	–	5–15
Plagioclase	25–40	30–50	45–50	35–45	45–60
Quartz	20–30	20–25	8–15	5–10	5–20
Amphibole	5–15	10–45	10–40	20–35	10–30
Biotite	rare	rare	–	–	rare
Clinopyroxene	–	–	–	15	–
Other minerals	Ap+Zrn+Ttn+Ep+ opaque	Ap+Zrn+Ttn+Ep+ Ilm+Mgt	Ap+Zrn+Ttn	Ttn+Ep+Ilm+Mgt	Ap+Zrn+Ttn+Ep+ Ilm+Mgt

deformational features (e.g. gneissosity, schistosity and foliation). The NW–SE trend is consistent with the compression of the rocks between the Arabia and Eurasia continents, corresponding to the closure of Neo-Tethys and the subsequent continental collision.

3. Petrography

The petrography of the granitoids and the associated migmatites is provided below. Modal amounts of minerals in the granitoids and migmatitic leucosomes are presented in Table 1. Mineral abbreviations are from Kretz (1983), except for amphibole (Amp).

The studied granitoids are classified as granodiorites, Qtz-monzodiorites and granites on the Streckeisen (1974) diagram.

Granodiorites. Coarse to medium granular texture is common in the granodiorites (Fig. 4a). The dominant mineral assemblage is plagioclase (30–50 modal %), K-feldspar (7–15 modal %), hornblende (10–45 modal %) and quartz (20–25 modal %). K-feldspar occurs as small subhedral laths and anhedral grains ranging from 0.2 to 0.4 mm in diameter. Plagioclase displays polysynthetic and Karlsbad twinnings.

Coarse-grained plagioclase exhibits optical zoning (Fig. 4a). Amphibole with greenish-brown to grey and olive-green pleochroism displays well-developed cleavages and is frequently twinned. In some hornblende crystals up to 2 cm in diameter, many zircons and opaque minerals occur as inclusions. Epidote, titanite and biotite are present in minor amounts. Magmatic epidote, in textural equilibrium with other magmatic phases, occurs as zoned and twinned crystals. Secondary epidote, replacing plagioclase, is seen sporadically in the rocks. Zircon, apatite and opaque minerals are accessory phases. Actinolite around hornblende is a late subsolidus crystallization product (Fig. 4b). Coarse-grained plagioclase and hornblende porphyroclasts in a fine-grained matrix are characteristics of the brecciated granodiorites (SW of Barut-Aghaji; Fig. 2). Plagioclase and quartz crystals show undulatory extinction.

Qtz-diorite. The mineral assemblage of the rock is plagioclase (35–45 modal %), hornblende (20–35 modal %), clinopyroxene (15 > modal %) and quartz

(5–10 modal %). Subhedral plagioclase (up to 4 mm in diameter) is weakly zoned and shows polysynthetic twinning. It is full of clinopyroxene inclusions and has a poikilitic texture. Clinopyroxene with a granular texture reaches up to 0.7 mm in diameter and is simply twinned. Amphibole is crystallized at the margins and parallel to the cleavage system of clinopyroxene (Fig. 4c). The magmatic hornblende (0.6 mm in length) is optically zoned and shows strong pleochroism. Euhedral titanite (up to 1.2 mm in diameter) and epidote are minor phases (Fig. 4d).

Qtz-monzodiorites. Plagioclase (45–50 modal %), hornblende (10–40 modal %) and K-feldspar (< 10 modal %) with a granular texture are the main constituent minerals of these rocks. Hornblende, 0.8 mm in diameter, is simply twinned and plagioclase (up to 5 mm in diameter) shows weak optical zoning. Titanite (0.4 mm in diameter) occurs in minor amounts. Apatite, zircon and opaque phases are accessory minerals.

Granites. Dominant minerals are quartz (20–30 modal %), plagioclase (25–40 modal %), K-feldspar (10–20 modal %) and hornblende (5–15 modal %). Granular texture is dominant in the granites. Hornblende reaches 1 mm in diameter. Plagioclase contains hornblende as inclusions. Titanite and biotite are minor phases. Accessory phases are zircon and apatite.

Mafic migmatites. Mafic migmatites occur in association with granitoids in the NW Ghar-e-Naz (Fig. 2; R. Hajialioghli, unpub. Ph.D. thesis, Univ. Tabriz, 2007). Structurally the investigated migmatites are very heterogeneous. Diatexite is the most common structure of the Takab mafic migmatites. Foliation in the mafic migmatites is marked by separation of the alternating centimetre-scale light-coloured quartz-feldspathic (leucosome) and dark hornblende-rich (melanosome) layers. Melanosome is also formed as thin selvages around leucosome. Schlieren structure includes floating melonocratic fragments in leucosome and is seen in some of the rocks (R. Hajialioghli, unpub. Ph.D. thesis, Univ. Tabriz, 2007). Migmatitic leucosomes have compositions consistent with granodiorite, Qtz-monzodiorite and Qtz-diorite. Medium-to fine-grained granular texture is common in the leucosomes. Subhedral plagioclase, 0.7 mm in diameter, is twinned (Fig. 4e). Quartz and K-feldspar occur with
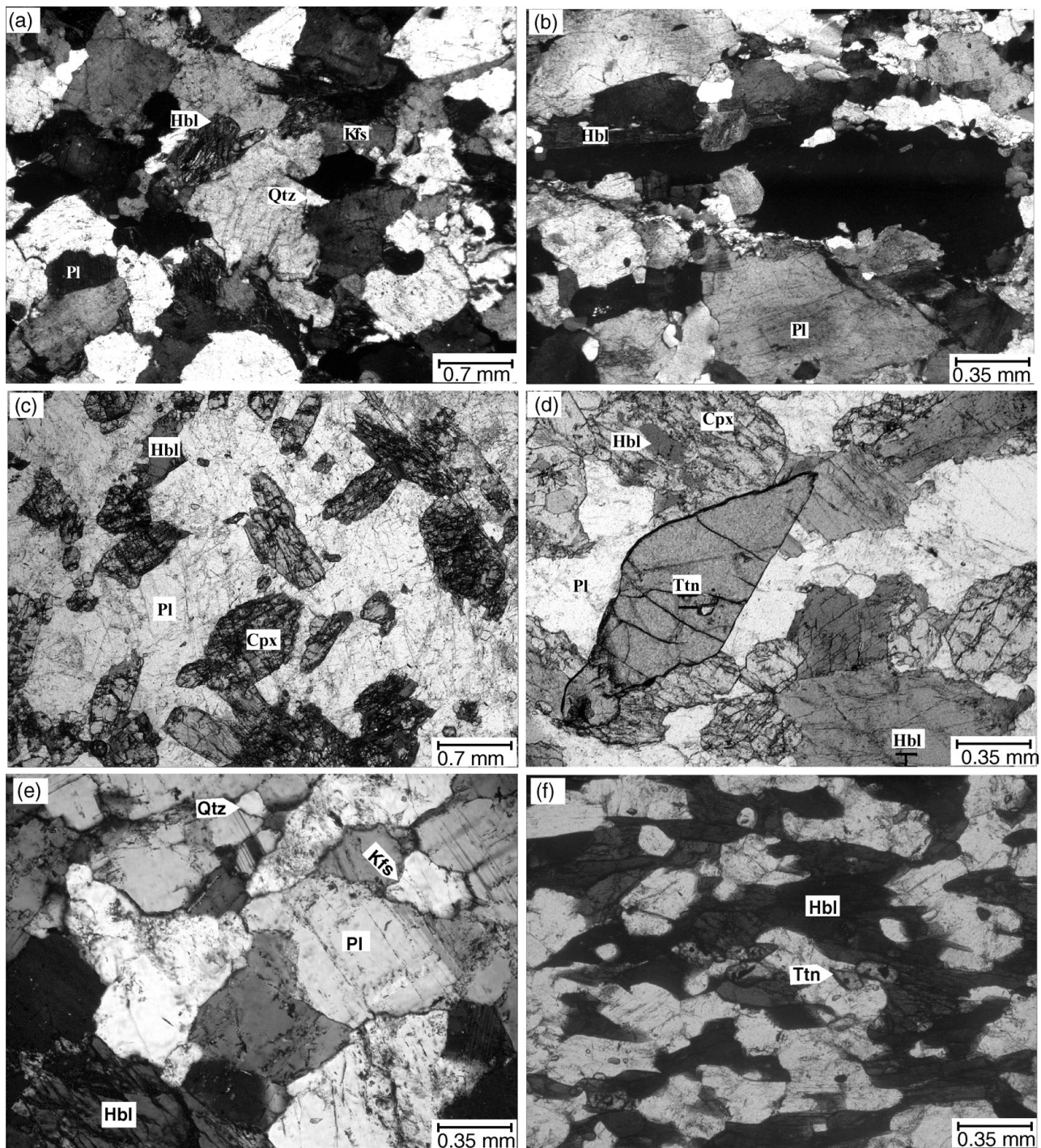
Figure 4. (a) Hornblende and plagioclase with granular texture in the granodiorite. Plagioclase shows compositional zoning. Crossed nicols, field of view 4.8 mm. (b) Subsolidus actinolite around magmatic hornblende in the granodiorite. Plain polarized light, field of view 2.4 mm. (c) Clinopyroxene, amphibole and plagioclase in the quartz diorite. Subsolidus amphibole is seen parallel to the cleavage system of clinopyroxene. Plain polarized light, field of view 2.4 mm. (d) Magmatic titanite in the diorite. Amphibole as patches within clinopyroxene and as products of deuteric alteration. Plain polarized light, field of view 2.4 mm. (e) The migmatitic leucosome with granular texture. Interstitial quartz and K-feldspar are anhedral. Plain polarized light, field of view 2.4 mm. (f) Hornblende and plagioclase with foliated texture in the mesosome. Plain polarized light, field of view 2.4 mm.

interstitial texture filling the spaces between plagioclase laths (Fig. 4e). Hornblende, biotite and titanite are present in minor amounts. Hornblende (> 50 modal %) and minor plagioclase are the essential minerals in the melanosome. The mesosome is characterized by foliated texture. It is composed of hornblende and plagioclase together with minor K-feldspar and quartz (Fig. 4f). Table 1 includes modal amounts of minerals of the mafic migmatites in the Takab area.

4. Analytical methods

Well-defined samples from the granitoids were analysed for major and trace elements at the

GeoForschungsZentrum, Potsdam, Germany. In addition, the leucosome, mesosome and melanosome portions of the migmatites were carefully separated and analysed for major oxides and trace elements. International rock standards were measured in the same runs to monitor the precision and accuracy of the XRF technique. The precision of the analyses is 1–3 % for the major element oxides and < 5 % for the trace elements. The results are presented in Table 2. FeO/Fe_2O_3 ratio is calculated using the conventional equation of Irvine & Baragar (1971) and SiO_2 v. (Na_2O+K_2O) diagram (Le Maitre, 1976). The amount of Fe_2O_3 is very low. Total iron is shown as Fe_2O_3 in Table 2.

Minerals from the granitoids were also analysed for major element oxides by wavelength-dispersive spectrometry using a CAMECA SX-100 microprobe at the GeoForschungsZentrum, Potsdam, Germany. The measuring conditions were 15 kv accelerating voltage, 10–20 nA beam current. The spot size was between 3 and 5 μm. A PAP correction procedure was applied. Natural and synthetic standards ((Fe_2O_3 (Fe)), rhodonite (Mn), rutile (Ti), MgO (Mg), wollastonite (Si, Ca), fluorite (F), orthoclase (Al, K) and albite (Na)) were used for the calibration of the element oxides. Representative mineral analyses are given in Table 3.

5. Whole-rock geochemistry

5.a. Major elements

Major element concentrations of the analysed rocks are listed in Table 2. The granitoids span a wide range of SiO_2 content (54–74 wt %). MgO, CaO, TiO_2 and FeO_t decrease with increasing SiO_2 content. Na_2O concentration of the granitoids is high at intermediate SiO_2 contents but it decreases toward more felsic compositions. CaO, Na_2O, TiO_2, MgO and Al_2O_3 variations versus SiO_2 in the leucosome part of migmatites show similar trends to those defined by these oxides in the granitoids.

Classification based on the normative Ab–Or–An scheme (Barker, 1979) identifies the analysed rocks as quartz monzonite, granodiorite and tonalite. On the total alkalis versus silica (TAS) diagram (Middlemost, 1994; Fig. 5a), the investigated granitoids are classified as granite, granodiorite, quartz monzonite, monzonite and quartz diorite. The rocks dominantly plot in the sub-alkaline field of the diagram of Irvine & Baragar (1971) (Fig. 5a). The agpaitic index (AI = mol (Na+K/Al)) shows that the samples are predominantly calc-alkaline (AI < 0.87; Liégeois & Black, 1987). Based on the discriminant diagram of Frost et al. (2001), the granitoids indicate alkali-calcic, calc-alkalic and calcic rock series (Fig. 5b). The analysed rocks have normative diopside, hypersthene and titanite, but normative corundum never exceeds 1 %. These features most likely characterize an I-type nature (Nagudi, Kobert & Kurat, 2003) for the source materials of the investigated granitoids.

The aluminium saturation index (ASI: molecular ratio of $Al_2O_3/(Na_2O+K_2O+CaO)$), ranging from 0.46 to 1.04, shows that the granitoids are metaluminous, comparable with migmatitic leucosome compositions (Fig. 5c). The diagram of $Al_2O_3/(Na_2O+K_2O)$ (A/NK) against $Al_2O_3/(CaO+Na_2O+K_2O)$ (A/CNK) also indicates a metaluminous characteristic for these rocks (Fig. 5d).

5.b. Trace elements

Trace element concentrations of the Takab granitoids and the associated migmatites are listed in Table 2, and their variations versus SiO_2 are plotted on Harker diagrams (Fig. 6). Sr concentration decreases, whereas Ba, Nb and Rb contents increase with increasing SiO_2 content. Zirconium shows a considerably scattered pattern (Fig. 6). Ni, Cr and V (transitional elements) exhibit a negative correlation with silica content since they behave as compatible elements. Samples from migmatitic leucosomes have compositional trends comparable with the trends for the granitoids.

The Rb/Zr–SiO_2 diagram (Harris, Pearce & Tindle, 1986) is used to discriminate I- and A-type granitoids from S-type rocks. The Takab granitoids and the migmatitic leucosomes plot mainly in the I- and A-type fields (Fig. 7a). The diagram of Zr versus SiO_2 (Collins et al. 1982) verifies the distinct I-type nature of these rocks (Fig. 7b).

The trace elements of the granitoids are normalized to primitive-mantle values (Sun & McDonough, 1989; Fig. 8). The composition of the leucosomes from the Takab area is also represented for comparison (Fig. 8). The trace element patterns of the different rock types show almost similar trends (Fig. 8). Nb and Ti show negative anomalies, but the Zr anomaly is positive.

6. Mineral chemistry

6.a. Feldspar

Representative electron microprobe analyses and the structural formula of plagioclase are given in Table 3. The plagioclase is zoned with core compositions of $X_{An} \sim 0.48$ and $X_{An} \sim 0.35$ and rim compositions of $X_{An} \sim 0.38$ and $X_{An} \sim 0.21$ in the quartz diorite and the granodiorite, respectively. The decrease of Ca from the core to the rim is interpreted as normal zoning during crystallization. The K_2O content of the plagioclase ranges between 0.03 and 0.05 (a.p.f.u.). The chemical compositions of plagioclase from granodiorite ($Ab_{63-79}An_{20-35}Or_{1-4}$) and quartz diorite ($Ab_{51-62}An_{38-48}Or_{1.0-1.5}$) are oligoclase and andesine, respectively.

6.b. Amphibole

Amphibole is the predominant mafic phase in the granitoids. Ferrous and ferric iron in the amphibole formula were calculated using the charge balance method. The

Table 2. Major and trace element compositions of the representative rocks in the Takab area

Rock type Sample	Gran. R29-w	Gran. R29-y	Gran. R17-A	Gran. R8-j	Gran. R17-c	Gran. R29-f	Gran. R8-k	Gran. R17-d	Gran. R3-1	Gran. R3-E	Gran. R51-A	Gran. R-3	Gran. R29-u	Leuc. R29-1	Leuc. R29-1	Leuc. R29-1	Meso. R29-1	Meso. R29-1	Meso. R29-1
SiO_2 (wt%)	54.10	56.50	56.6	57.80	58.2	59.30	61.70	62.5	65.7	66.0	68.20	69.1	73.90	54.2	54.2	63.3	46.7	46.9	48.7
TiO_2	0.45	0.69	0.73	0.71	0.23	0.56	0.15	0.63	0.33	0.53	0.35	0.19	0.10	0.52	0.50	0.61	1.71	1.22	1.14
Al_2O_3	22.10	19.30	16.7	18.60	12.3	18.20	22.00	15.4	17.60	15.20	16.30	15.6	14.50	24.0	22.0	17.4	18.5	18.5	17.3
$Fe_2O_3{}^*$	4.45	4.87	7.77	5.64	7.95	4.34	0.84	5.94	1.95	4.25	1.82	1.56	0.28	3.51	5.06	3.70	11.11	10.91	11.71
MnO	0.10	0.09	0.14	0.11	1.26	0.09	0.02	0.10	0.04	0.07	0.05	0.04	0.01	0.09	0.10	0.08	0.21	0.29	0.23
MgO	2.77	2.03	4.58	1.68	3.37	2.40	0.39	3.64	0.83	2.53	0.54	0.51	0.16	1.46	2.05	1.83	5.4	5.4	5.17
CaO	8.79	5.91	8.52	6.10	8.07	8.01	4.76	6.5	4.23	5.96	3.33	2.16	1.75	8.87	8.14	6.66	8.23	10.31	9.05
Na_2O	5.44	5.68	3.05	5.99	3.25	4.11	7.97	3.85	5.31	4.03	4.45	3.52	2.84	5.52	5.71	4.15	3.09	3.38	4.1
K_2O	0.45	2.72	0.48	1.58	3.59	0.99	0.75	0.26	2.53	0.22	3.72	5.93	5.62	0.39	0.45	0.75	2.31	0.7	0.59
P_2O_5	0.07	0.37	0.10	0.37	0.01	0.55	0.08	0.14	0.14	0.14	0.14	0.10	0.04	0.20	0.16	0.19	0.30	0.40	0.29
CO_2	0.07	0.39	0.04	0.04	0.03	0.16	0.06	0.04	0.05	0.04	0.05	0.04	0.04	0.05	0.07	0.1	0.11	0.06	0.04
H_2O	0.96	0.76	1.06	1.07	1.15	1.03	1.06	0.91	1.05	0.83	0.79	0.89	0.54	0.91	1.17	0.97	1.81	1.52	1.49
Sum	99.75	99.31	99.77	99.69	99.41	99.74	99.78	99.91	99.76	99.80	99.74	99.64	99.78	99.72	99.61	99.74	99.48	99.59	99.72
Ba (ppm)	112	2396	78.0	432	4824	291	92.0	130	661	142	875	1277	1778	151	141	220	621	103	125
Cr	14.0	< 10	57.0	< 10	23.0	29.0	11.0	113	< 10	47.0	< 10	< 10	< 10	12.0	19.0	28.0	120	255	40.0
Ga	22.0	18.0	18.0	22.0	10.0	20.0	21.0	17.0	16.0	15.0	16.0	16.0	13.0	21.0	19.0	19.0	22.0	24.0	18.0
Nb	6.00	13.0	2.00	14.0	5.00	12.0	13.0	< 2.0	15.0	6.00	28.0	15.0	13.0	6.00	5.00	15.0	21.0	12.0	6.00
Ni	22.0	< 10	23.0	< 10	38.0	17.0	< 10	35.0	< 10	15.0	< 10	< 10	< 10	16.0	14.0	23.0	101	98.0	28.0
Rb	< 10	10.0	< 10	< 10	31.0	< 10	< 10	< 10	37.0	< 10	73.0	106	79.0	< 10	< 10	< 10	51.0	< 10	< 10
Sr	990	1924	187	891	325	698	1064	267	488	324	449	444	473	1083	989	703	545	643	619
V	86.0	107	192	84.0	73.0	91.0	22.0	134	30.0	110	43.0	35.0	12.0	61.0	121	78.0	279	187	385
Y	14.0	21.0	21.0	19.0	18.0	18.0	< 10	24.0	20.0	19.0	34.0	12.0	10.0	12.0	14.0	19.0	39.0	36.0	28.0
Zn	63.0	62.0	67.0	77.0	103	64.0	10.0	49.0	24.0	43.0	25.0	21.0	4.00	39.0	51.0	56.0	174	143	115
Zr	85.0	211	94.0	187	195	94.0	136	133	204	136	115	148	90.0	262	199	198	226	116	70.0
Norm(wt%)Ilm	0.86	1.32	1.38	1.34	0.45	1.06	0.05	1.20	0.09	1.00	0.11	0.09	0.03	0.36	0.95	0.41	3.25	2.32	2.17
Ttn	0.00	0.00	0.00	0.00	0.00	0.00	0.30	0.00	0.69	0.00	0.70	0.35	0.00	0.82	0.00	0.96	0.00	0.00	0.00
Di	6.74	5.10	8.90	7.16	27.17	5.64	0.47	5.79	1.82	4.55	0.85	0.35	0.00	1.58	4.72	2.70	6.8	12.19	13.45
Hy	2.22	3.03	13.39	3.54	6.47	4.10	0.76	9.64	1.22	4.79	0.95	1.11	0.40	2.90	3.60	3.31	0.00	0.00	0.00
Ol	2.19	0.77	0.00	0.00	0.00	0.00	0.00	0.00	0.00	0.00	0.00	0.00	0.00	0.00	0.00	1.27	0.00	13.2	13.74
ASI=Al/Na+K+Ca	0.87	0.84	0.79	0.82	0.51	0.81	0.97	0.83	0.92	0.86	0.94	0.97	1.04	0.94	0.89	0.88	0.82	0.74	0.72
AI=Na+K/Al	0.43	0.63	0.30	0.62	0.33	0.43	0.63	0.75	0.65	0.45	0.69	0.78	0.74	0.43	0.45	0.39	0.41	0.34	0.43

Gran. – Granitoid; Leuc. – Leucosome; Meso. – Mesosome. *Fe total as Fe_2O_3.

Table 3. Representative mineral analyses from the Takab granitoids

Mineral	Quartz diorite (sample R29-G)														Granodiorite (sample R-51-A)				
	Amp	Amp core	Amp rim	Pl	Pl rim	Pl core	Cpx	Cpx	Cpx	Ttn	Ttn	Ilm	Amp core	Amp rim	Amp	Pl core	Pl	Pl rim	Ep
SiO_2	45.48	44.40	46.07	55.74	58.74	55.76	50.49	54.21	53.71	29.92	30.64	0.00	44.17	46.02	48.58	59.03	62.96	62.16	36.50
TiO_2	1.63	5.38	0.58	0.00	0.02	0.04	0.26	0.24	0.08	36.80	38.28	53.01	1.07	0.44	0.24	0.01	0.01	0.00	0.06
Al_2O_3	10.47	7.44	10.57	29.14	27.23	29.09	6.43	0.35	1.41	1.54	1.41	0.00	10.05	8.28	6.11	26.53	24.43	24.54	22.69
Cr_2O_3	0.23	0.19	0.19	0.06	0.00	0.00	0.16	0.01	0.06	0.00	0.00	0.00	0.00	0.01	0.01	0.00	0.00	0.01	0.00
FeO	14.03	12.97	14.23	0.08	0.06	0.01	13.48	6.57	7.87	1.47	0.71	29.97	17.91	18.30	17.23	0.07	0.07	0.01	0.00
MnO	0.27	0.26	0.27	0.01	0.01	0.00	0.32	0.31	0.31	0.10	0.07	17.05	0.49	0.49	0.50	0.00	0.00	0.00	0.17
MgO	13.20	11.84	13.45	0.00	0.00	0.00	15.59	15.51	14.52	0.00	0.00	0.03	11.17	11.58	12.79	0.00	0.01	0.00	0.03
CaO	11.94	14.30	12.20	10.35	8.37	10.49	12.66	24.52	23.83	27.05	27.89	0.00	11.53	11.72	11.81	7.61	4.84	4.83	23.11
Na_2O	1.38	0.72	1.20	6.04	7.49	6.20	0.72	0.22	0.50	0.00	0.00	0.00	1.46	1.02	0.90	7.69	9.46	9.70	0.00
K_2O	1.05	0.67	1.02	0.19	0.18	0.18	0.31	0.01	0.00	0.00	0.00	0.00	1.19	0.70	0.44	0.28	0.20	0.18	0.00
Sum	99.60	98.47	99.81	101.60	102.00	101.77	100.42	101.71	102.00	96.88	99.00	100.05	99.00	98.50	98.60	101.20	101.90	101.40	96.90
F	0.15	0.26	0.12	0.27	0.00	0.14	0.24	0.19	0.28	0.00	0.00	0.00	0.51	0.29	0.17	0.03	0.08	0.17	0.07
Cl	0.04	0.04	0.03	0.00	0.00	0.00	0.03	0.00	0.00	0.00	0.00	0.00	0.03	0.01	0.02	0.00	0.01	0.03	0.00
(O)	23	23	23	8	8	8	6	6	6	5	5	3	23	23	23	8	8	8	12.50
Si	6.51	6.57	6.56	2.47	2.58	2.74	1.86	1.97	1.95	1.00	1.00	0.00	6.46	6.73	7.03	2.61	2.74	2.74	2.94
Al	1.76	1.33	1.77	1.52	1.41	1.52	0.28	0.02	0.05	0.06	0.05	0.00	1.73	1.42	1.04	1.38	1.25	1.25	2.13
Fe^{3+}	0.61	0.00	0.72	0.00	0.00	0.00	0.05	0.07	0.08	0.04	0.02	0.00	0.86	0.95	0.86	0.00	0.00	0.00	0.95
Fe^{2+}	1.07	1.64	0.97	0.00	0.00	0.00	0.37	0.13	0.16	0.00	0.00	0.65	1.33	1.28	1.23	0.00	0.00	0.00	0.00
Ti	0.17	0.60	0.06	0.00	0.00	0.00	0.01	0.01	0.00	0.93	0.95	1.00	0.12	0.05	0.03	0.00	0.00	0.00	0.00
Cr	0.03	0.02	0.02	0.00	0.00	0.00	0.00	0.00	0.00	0.00	0.00	0.00	0.00	0.00	0.00	0.00	0.00	0.00	0.00
Mn	0.03	0.03	0.03	0.00	0.00	0.00	0.01	0.01	0.01	0.00	0.00	0.34	0.06	0.06	0.06	0.00	0.00	0.00	0.01
Mg	2.82	2.61	2.85	0.00	0.00	0.00	0.86	0.84	0.79	0.00	0.00	0.00	2.44	2.51	2.76	0.00	0.00	0.00	0.00
Ca	1.83	2.27	1.86	0.49	0.39	0.50	0.50	0.95	0.93	0.98	0.99	0.00	1.81	1.83	1.83	0.36	0.23	0.22	1.97
Na	0.38	0.21	0.33	0.52	0.64	0.53	0.05	0.02	0.03	0.00	0.00	0.00	0.41	0.29	0.25	0.66	0.80	0.82	0.00
K	0.19	0.13	0.18	0.01	0.01	0.01	0.01	0.00	0.00	0.00	0.00	0.00	0.22	0.13	0.08	0.02	0.01	0.01	0.00
Sum	15.40	15.37	15.38	5.02	5.03	5.03	4.00	4.02	4.00	3.01	3.01	1.99	15.44	15.25	15.16	5.03	5.03	5.04	8.00
$Al^{[IV]}$	1.49	1.29	1.44	–	–	–	0.14	0.02	0.05	0.00	0.00	–	1.54	1.27	0.97	–	–	–	–
$Al^{[VI]}$	0.27	0.03	0.33	–	–	–	0.14	0.00	0.00	0.01	0.05	–	0.19	0.15	0.07	–	–	–	0.06
Mg/Mg+Fe	0.72	0.61	0.75	–	–	–	0.94	0.92	0.79	–	–	–	0.65	0.66	0.69	–	–	–	2.07
$Al/Al+Fe^{3+}+Cr^{3+}$	0.73	0.98	0.71	–	–	–	0.85	0.22	0.12	–	–	–	0.67	0.60	0.55	–	–	–	–
$(K+Na)_A$	0.41	0.34	0.38	–	–	–	–	–	–	–	–	–	–	–	–	–	–	–	0.69
Na/Na+K+Ca	0.16	0.08	0.14	0.51	0.61	0.51	0.09	0.02	0.03	0.00	0.00	–	0.09	0.13	0.12	0.64	0.77	0.77	–
K/Ca+K+Na	0.08	0.05	0.08	0.01	0.01	0.01	0.02	0.00	0.00	0.00	0.00	–	0.17	0.06	0.03	0.02	0.01	0.01	–
Ca/K+Na+Ca	0.76	0.87	0.78	0.48	0.38	0.48	0.89	0.98	0.97	1.00	0.00	–	0.74	0.81	0.85	0.35	0.22	0.22	–

Amp – amphibole; Pl – plagioclase; Cpx – clinopyroxene; Ttn – titanite; Ilm – ilmenite; Ep – epidote.
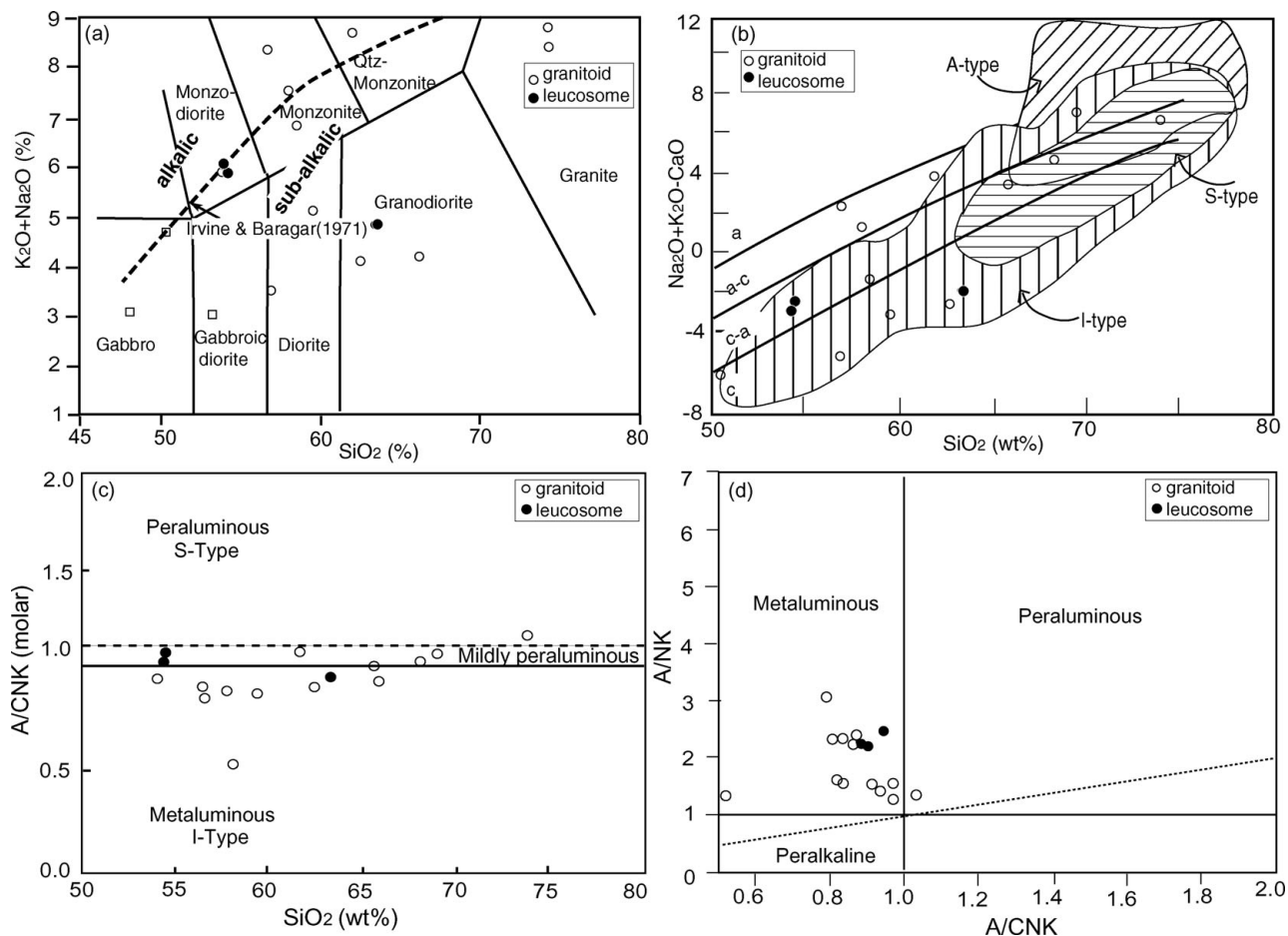
Figure 5. Geochemical classification of the granitoids. (a) Total alkalis v. silica diagram (Middlemost, 1994). (b) Major element discrimination diagrams of Frost *et al.* (2001). The analysed rocks range from alkali-calcic, calc-alkali to calcic rock series. (c) A/CNK v. SiO_2 (wt %) diagram (Chappell & White, 1974). (d) Plot of A/NK v. A/CNK for the granitoids and migmatitic leucosome in the Takab area. A/NK = molar ratio of $Al_2O_3/(Na_2O+K_2O)$; A/CNK = molar ratio of $Al_2O_3/(CaO+Na_2O+K_2O)$. The analysed rocks indicate dominantly metaluminous characteristics. The leucosome compositions are presented for comparison.

amphiboles are calcic using the classification of Leake *et al.* (1997) $((Ca+Na)^{(M4)} \geq 1.34;\ Na^{(M1)} < 0.67)$. Core compositions are different, having higher TiO_2 content. Hornblende inclusions in plagioclase have chemical compositions indistinguishable from the core compositions of the hornblende within the rock. The Ti content of amphiboles from the granodiorite is low compared to that of the quartz diorite. On the classification diagram of Leake *et al.* (1997), the amphibole compositions are consistent with tschermakite and hornblende with minor amounts of edenite and tremolite end-members. Secondary tremolite has high Mg and Si and low Al contents.

6.c. Clinopyroxene

Representative clinopyroxene analyses from the quartz diorite are shown in Table 3. The clinopyroxene has mainly high MgO (14.50–15.60 wt %), FeO (6.5–13.5 wt %) and CaO (12.60–24.60 wt %) concentrations but it is low in TiO_2 (< 0.26 wt %) and Na_2O (< 0.75 wt %) contents. In the classification diagram of Morimoto *et al.* (1988), the analysed clinopyroxenes plot in the 'Quad' field. Their compositions vary

in the range of $En_{42-44}Fs_{7-9}Wo_{48-50}$. Clinopyroxene compositions on En–Fs–Wo diagram (after Deer, Howie & Zussman, 1978) are diopside. On the basis of the Ti content, clinopyroxenes from the Takab area plot in the low- and very low-Ti field of the diagram by Beccaluva *et al.* (1989). Plotting on diagrams of Ti (a.p.f.u.) against Ca+Na (a.p.f.u.) and Al_2O_3 against silica content (Fig. 9) shows a sub-alkaline character for the quartz diorite.

6.d. Titanite

Analysed titanite from the quartz diorites has Ti and Ca contents of 0.94 (a.p.f.u.) and 0.99 (a.p.f.u.), respectively. Al concentration is also low (0.06 a.p.f.u.). ZnO and Cr_2O_3 contents are very low (0.07 and 0.05 to 0.10 wt %, respectively).

6.e. Epidote

The structural formula is calculated for 8 cations and 12.5 oxygens (Table 3). All iron is considered as Fe^{3+}. Al occupies the tetrahedral site only in small amounts (up to 0.06 a.p.f.u.). $Al^{VI}/(Al^{VI}+Fe^{3+})$ is 0.69. The
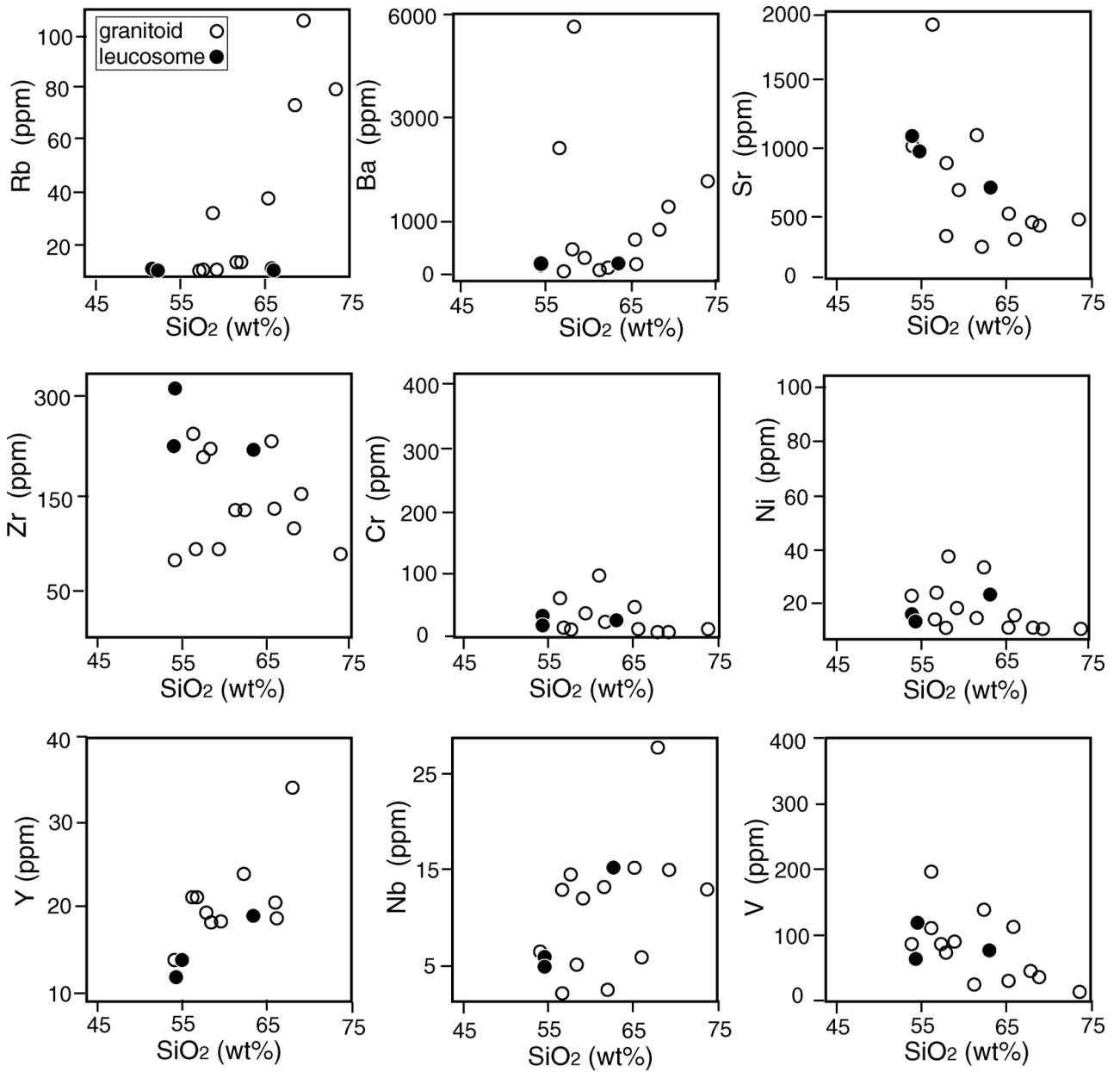
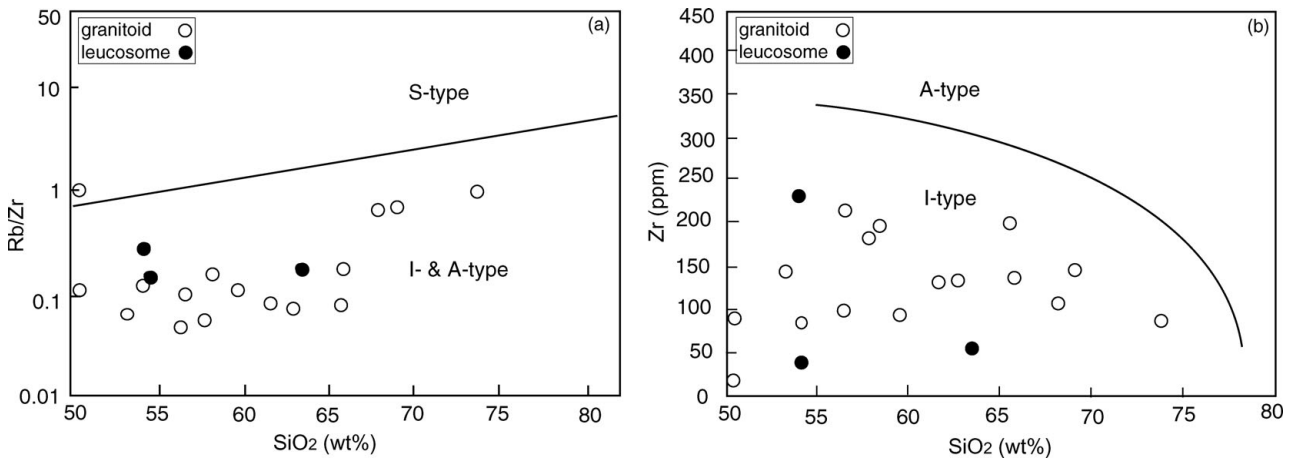Figure 6. Trace element variations for the granitoids from the Takab area. For details see text.

Figure 7. (a) Rb/Zr v. SiO$_2$ diagram (Harris, Pearce & Tindle, 1986) discriminating I-and A-types granitoids from S-type rocks. (b) Zr v. SiO$_2$ diagram of Collins *et al.* (1982). Both verify I-type nature for the analysed rocks.
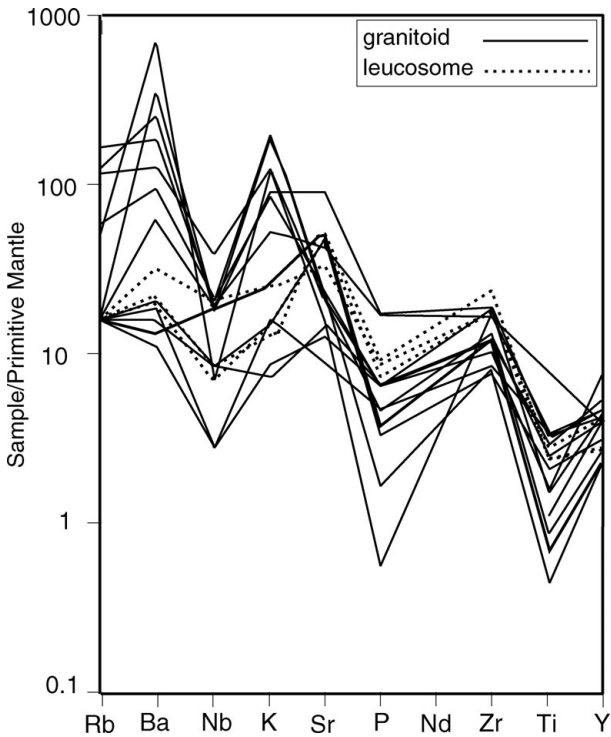
Figure 8. Primitive mantle-normalized element patterns for the granitoids from the Takab area. Normalization factors are after Sun & McDonough (1989). The migmatitic leucosome compositions are presented for comparison.

mean composition of the end-members in the analysed epidote from the granodiorite is $Cz_{11}Ep_{79}Fe–Ep_{10}$.

6.f. Ilmenite

The structural formula is calculated on the basis of 2 cations and 3 oxygens (Table 3). All iron is considered as Fe^{2+}. Ilmenite ($FeTiO_3$) and pyrophanite ($MnTiO_3$) are the dominant end-members, whereas the end-member geikielite ($MgTiO_3$) is absent. The mean composition of the analysed ilmenite from the quartz diorite is $Ilm_{63}Prh_{36}$.
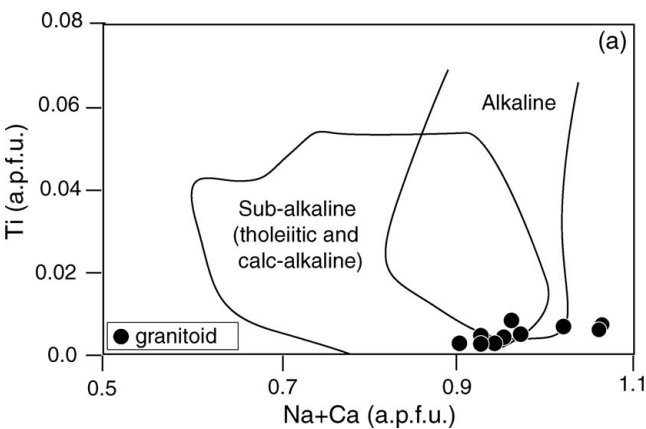
Table 4. Mole fraction and ideal activity expressions used for clinopyroxene geobarometry in the quartz diorite

Clinopyroxene activity–composition relationships (Wood, 1979)

Cation assignment (recalculated on the basis of 6 oxygens)
$Al^{IV} = 2−Si$
$X^{M1}Al = Al^{−IV}Al$
$X^{M2}Ca = Ca$
$X^{IV}Si = Si/2$
$X^{IV}Al = (2−Si)/2$
$a_{CaTs}Cpx = 4.X^{M2}Ca.X^{M1}Al.X^{IV}Al.X^{IV}Si$
Plagioclase activity–composition relationships (Holland & Powell, 1992)
$X_{An} = Ca/(Ca+Na+K)$
$X_b = 0.12+0.00038.T$
$X_{An(2Tmodel)} = [X_{An}(1+XAn)^2 1]/4$
$I_{An} = −RTLn(X_{An(2T)}/X_{An})−(W_c−W_i)91−X_b)^2$
$W_c = 1070.0$ J mol^{-1}, $W_i = 9790.0$ Jj mol^{-1}
$a_{An(2T)}{}^{Pl} = X_{An(2T)}.exp\{1/RT[W_c(1−X_{An})^2+I_{An}]\}$

T – temperature in K.

7. Magmatic and subsolidus pressures and temperatures estimates

The composition of clinopyroxene was used to determine the crystallization pressure in quartz diorite, based on the McCarthy & Patiño Douce (1998) barometer which is calibrated for *P–T* ranges of ≥ 4 kbar and ≥ 700 °C. The crystallization pressure obtained for the quartz diorite is 7.8 (± 2.5) kbar, which is consistent with a depth of about 24 km, reflecting crystallization at a crustal level. The activity of the Ca-tschermak component in clinopyroxene was calculated with the ideal activity model. Table 4 shows mole fraction and ideal activity expressions used for pressure estimations by the clinopyroxene barometer of McCarthy & Patiño Douce (1998).

The significant exchange vector for amphiboles from the Takab granodiorites is $Al_2^{IV}\square^A Mg^{VI}Si^{IV}$ $(Na,K)_{−1}{}^A(Fe^{3+}, Al)_{−1}{}^{VI}$ indicating a combination of both the pressure- and temperature-sensitive substitutions. Applying the Al in amphibole barometers of Hollister *et al.* (1987) and Johnson & Rutherford (1989) (considering the proper amphibole formula
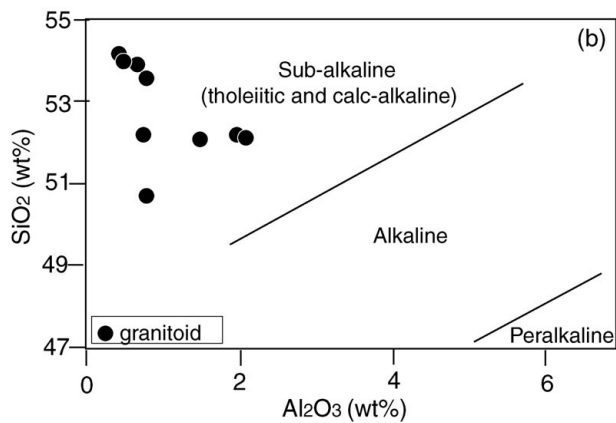

Figure 9. (a) Ti (a.p.f.u.) against Na+Ca (a.p.f.u.) diagram (Leterrier *et al.* 1982). (b) Sub-alkaline characteristic of the granitoids on the SiO_2 (wt %)–Al_2O_3 (wt %) diagram. The positions of boundaries between sub-alkaline, alkaline and peralkaline magma types are from Le Bas (1962).

Table 5. Estimated temperatures and pressures for the Takab granitoids

Sample number	Representative rock type	Magmatic crystallization	Subsolidus re-equilibrium
R51-A	Granodiorite	$T \sim 790 + 75\,°C$ (B&H), 700 °C (O) $P \sim 4.8(\pm3)$ kbar (H&Z), $5(\pm1)$ kbar (H), 4.3 kbar (J&R)	$T \sim 620\,°C$ (O) $P \sim 3.6(\pm3)$ kbar (H&Z), $3.6(\pm1)$ kbar (H), 3.3 kbar (J&R)
R29-G	Qtz-diorites	$T \sim 820 \pm 75\,°C$ (B&H), 760 °C (O) $P \sim 7.8(\pm2.5)$ kbar (M&P)	$T \sim 600\,°C$ (O) $P \sim 5.6(\pm3)$ kbar (H&Z), $6(\pm1)$ kbar (H), 5.1 kbar (J&R)

B&H – Blundy & Holland, 1990; O – Otten, 1984; H&Z – Hammarstrom & Zen, 1986; H – Hollister *et al.* 1987; M&P – McCarthy & Patiño Douce, 1998; J&R – Johnson & Rutherford, 1989.

calculation for 13eCNK cations (13 cations excluding Ca, Na, and K) and 23 oxygens) yields crystallization pressure of $P \sim 5\ (\pm1)$ kbar (Hollister *et al.* 1987) and $P \sim 4.3\ (\pm1)$ kbar (Johnson & Rutherford, 1989) for the granodiorites. The aluminium in the amphibole geobarometer of Hammarstrom & Zen (1986) gives a pressure of 4.8 (±3) kbar. The estimated crystallization pressure for the granodiorites is consistent with the emplacement at a depth of about 13–15 km. Within the uncertainty limits of the estimated pressures, the existence of primary magmatic epidote in the paragenesis of the Takab granodiorites and quartz diorites supports the estimated pressures, since epidote in magmatic rocks crystallizes at 6–8 kbar (e.g. Naney, 1983; Zen & Hammarstrom, 1984, 1988). Subsolidus recrystallization pressure of the quartz diorite is determined using the Al barometer for the composition of the secondary amphibole, which grows around clinopyroxene. It is about 5 kbar (Table 5). Al barometry for the amphibole rim composition of the granodiorite yields a subsolidus pressure of about 3 kbar (Table 5).

Crystallization temperatures of the investigated rocks were calculated for the core composition of the amphiboles, using the plagioclase–amphibole calibration of Blundy & Holland (1990) as a reliable method for geothermometry of granitoids (Moazzen & Droop, 2005), given that the reported uncertainty for Blundy & Holland's (1990) calibration is ± 75 °C (T ∼ 850 °C ± 75 °C for the quartz diorites and T ∼ 790 °C ± 75 °C for the granodiorites). Estimated temperatures using the Ti content of amphibole, calibrated by Otten (1984), are consistent with crystallization at $T \sim 760\,°C$ and $T \sim 700\,°C$ for the quartz diorite and the granodiorite, respectively. The Ti content of the analysed amphiboles in the quartz diorite and the granodiorite decreases towards the rim. The Ti content of amphibole rims using the Otten (1984) method gives subsolidus temperatures of 620 °C and 600 °C for the quartz diorites and the granodiorites, respectively. A study by Stern, Huang & Wyllie (1975) showed that the solidus temperature for andesitic melt is about 700 °C at 3 kbar under water-saturated conditions. Since the studied rocks here are more mafic than andesite, it is more likely that they had higher solidus temperatures, therefore the calculated temperatures indicate subsolidus re-equilibration conditions.

8. Discussion and conclusions

Mineralogical characteristics (Ishihara, 1977; Whalen & Chappell, 1988; Vyhnal, McSween & Speer, 1991) were used to verify the I-type magmatic series for the Takab granitoids. Some obvious mineralogical indications supporting the I-type character of the Takab granitoids are: (1) amphibole is the dominant constituent mafic mineral, (2) minor titanite and epidote occur in textural equilibrium with plagioclase and hornblende with a granular texture, (3) magnetite and ilmenite are the accessory opaque phases, (4) Al-rich mineral phases such as garnet and muscovite are absent in the investigated rocks, (5) the modal percentage of plagioclase is greater than K-feldspar and quartz.

The granitoids show a low aluminium saturation index (ASI), low concentration of SiO_2 and high FeO, MgO and CaO contents, which are typical features for I-type granitoids. The K_2O content varies from low-K to high-K series (Rickwood, 1989). The low K_2O content in some of the analysed granitoids can be explained by the K_2O-poor nature of the source. Low Nb, Y, K_2O values and $FeO_t/(FeO_t+MgO) < 0.75$ for the granitoids in the Takab area are analogous values to those of calc-alkaline rocks (Guimarães *et al.* 1998; Guimarães & Da Silva Filho, 2000).

Furthermore, the high-Si and low-Ti contents of the analysed clinopyroxenes characterize the sub-alkaline nature of the magmatic rocks (e.g. Nisbet & Pearce, 1977; Moazzen & Oberhansli, 2008). This feature may have two interrelated explanations: (1) high $aSiO_2$ in the sub-alkaline magma causes a high proportion of Si and hence a low proportion of Al in the tetrahedral site of clinopyroxene, the charges being balanced by a low proportion of Ti in the octahedral site (Nisbet & Pearce, 1977); (2) low contents of Ti may reflect the crystallization history of the melt (probably the earlier crystallization of pyroxene in relation to plagioclase or early crystallization of magnetite and/or slow rates of cooling: e.g. Nisbet & Pearce, 1977). Ti and Al contents of clinopyroxene are related to the silica activity of the melt from which they crystallized (Kushiro, 1960; Le Bas, 1962). Therefore, low Ti contents in the analysed clinopyroxenes may characterize silica-saturated sub-alkaline magmas (Verhoogen, 1962).

The geochemical variations of the Takab granit-oids indicate that they were probably generated by

fractionation of basic to intermediate calc-alkaline compositions (e.g. Hall, 1987; Opiyo-Akech, Tarney & Hoshino, 1999). The overall decrease in FeO_t and MgO contents of the Takab granitoids while SiO_2 increases can be related to the fractionation of the mafic minerals, mainly hornblende. The Mg no. (Mg/(Mg+Fe)) of the granitoids, ranging from 25 to 65, may support this. Compatible elements such as Cr and Co are strongly depleted in the silicic rocks, indicating lower abundance of mafic minerals (Fig. 6). The decrease of TiO_2 content in the silicic compositions is more likely due to crystallization of accessory minerals such as titanite/rutile from the melt. The decrease of V content with increasing SiO_2 (Fig. 6) suggests fractionation of Fe–Ti oxides. Negative correlation between Ca and Sr versus SiO_2 indicates crystallization of plagioclase during differentiation. The steady increase in Rb and K_2O concentrations precludes alkali feldspar fractionation in the intermediate compositions. The P_2O_5 versus SiO_2 array displays an abrupt change in concentration of P_2O_5 in the intermediate compositions, which may be explained by the crystallization of apatite. The variation of Zr content, with respect to SiO_2 variation, is not systematic (Fig. 6).

The major and trace element behaviour for the migmatitic leucosomes is similar to the trends defined by the granitoids (Fig. 6).

Primitive mantle normalized trace element patterns for the Takab granitoids are shown in Figure 8. The leucosome composition is also plotted to compare the results. Ba anomalies and relatively high K in these sets of rocks (Fig. 8) can be attributed to release of these elements from hornblende and/or rare K-feldspar in the source materials during partial melting (Rollinson, 1993). The Sr anomaly probably indicates contribution of plagioclase as a dominant phase in the magma evolution. Negative anomalies of P and Ti indicate involvement of apatite and rutile as residual phases in the magma source. Negative Nb and Ti anomalies in the rocks can be considered as characteristic of the crustal source and/or subduction-related magmatic effects, that is, fluids (or melts) derived from subducted sediments (Saunders, Tarney & Weaver, 1980).

8.a. Tectonic setting

In order to find the tectonic setting for the granitoid magmatism in the Takab area, the compositions of the granitoids and the leucosomes of migmatites are plotted on appropriate diagrams. Both the granitoids and leucosome parts of the migmatites show affinities with volcanic arc granitoids (VAG) and syn-collisional granitoids (syn-COLG) (Fig. 10a, b). The same result is reached on the basis of major elements (FeO, MgO and CaO wt %; Maniar & Piccoli, 1989), indicating geochemical affinities similar to volcanic arc and collisional granitoids (Fig. 10c). Most of the granitoids and migmatitic leucosomes plot in the collision field of the Zr versus (Nb/Zr)N diagram of Thiéblemont & Tégyey (1994) (Fig. 10d). The collisional setting for

the studied granitoids cannot be proved unequivocally and the volcanic arc origin cannot be ruled out easily, but considering what is shown in Figure 10d, a collisional setting for them is more likely. In addition, the geochemical volcanic arc features can be attributed to the nature of the materials inherited from previous arc-related protoliths.

8.b. Crustal source material

Some field geological features such as the limited volume of the granitoids and the lack of mantle xenoliths, as well as the existence of metabasic enclaves in the magmatic rocks and existence of the mafic migmatites, lead to the proposition that the investigated granitoids generated from partial melting of a crustal source and are not mantle derived.

Chemically, the crustal source for the investigated granitoids is deduced from their Nb/Y versus Rb/Y data (Fig. 11a). The granitoids in the study area have predominantly low Rb/Nb values (0.3–3.0) and plot close to the lower crust values (Rudnick & Fountain, 1995) (Fig. 11a). High concentrations of CaO, MgO and FeO_t and low K_2O/Na_2O values classify the source of the investigated rocks as metabasites. To constrain the source material, they were plotted in the partial melts from the metabasaltic source field diagram of Altherr & Siebel (2002) (Fig. 11b–d). The ternary plot of $CaO–ASI/30–2K_2O$ (molar) (Christofides *et al.* 2007) verifies the results.

8.c. Tectonic model for the Takab complex

Geological and lithological characteristics of the Takab metamorphic complex show affinities to the Central Iran micro-continent (Hajialioghli *et al.* 2007a). An intrusion age of the gneiss in the Takab complex is dated at 560 Ma (U/Pb zircon: Stockli *et al.* 2004), which is similar to a U/Pb date from basement rocks of the Saghand area in the Central Iran Zone (Ramezani & Tucker, 2003), related to the Pan-African orogeny. Migmatization of the metamorphic rocks in both the Takab area (U/Pb zircon dating, *c.* 25 Ma: R. Hajialioghli, unpub. Ph.D. thesis, Univ. Tabriz, 2007; Moazzen & Hajialioghli, 2008) and the Central Iran Zone (U/Pb zircon dating, *c.* 40 Ma: Ramezani & Tucker, 2003) occurred in relation to the Alpine orogeny. If, as we have argued, the Takab metamorphic basement correlates with equivalent rocks in the Central Iran Zone, it seems reasonable to compare granitoids in the study area with those in the Central Iran Zone related to the subduction of Neo-Tethys oceanic crust during Alpine orogeny. Considering the field evidence as well as U/Pb isotope geochemistry ages of the mafic migmatites from the Takab area (*c.* 25 Ma; R. Hajialioghli, unpub. Ph.D. thesis, Univ. Tabriz, 2007), a Tertiary age for the Takab granitoids is very likely. Although the accurate timing of collision between the Arabian plate and the Iranian block and associated magmatic activity is highly controversial
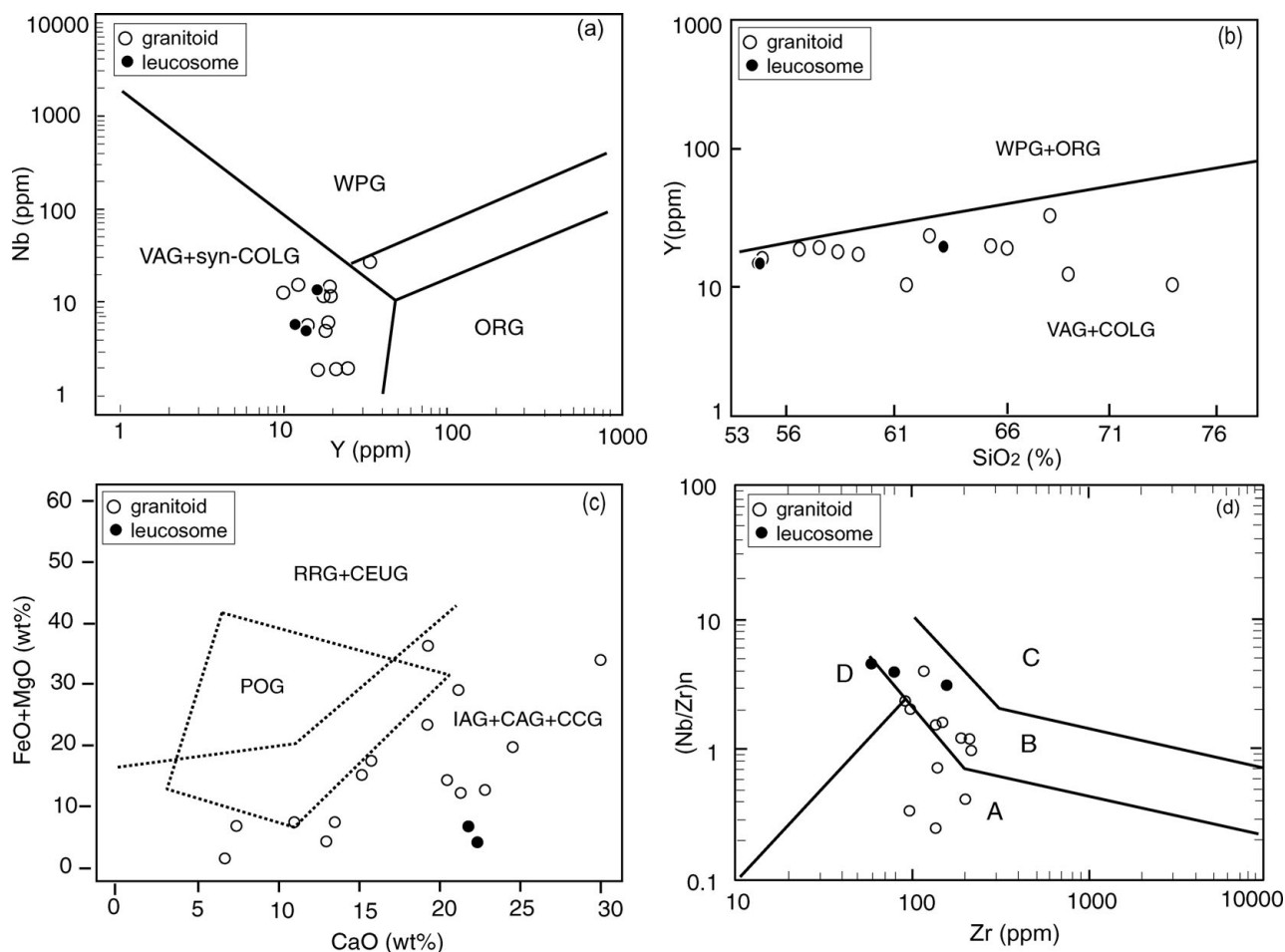
Figure 10. (a, b) Discrimination diagrams of Y v. Nb and SiO v. Y (wt %) (after Pearce, Harris & Tindle, 1984) classify the Takab granitoids as volcanic arc and syn-collisional rocks. VAG – volcanic arc granitoids; COLG – collisional granitoids; syn-COLG – syn-collisional granitoids; ORG – ocean ridge granitoids; WPG – within-plate granitoids. (c) Major discrimination diagram of Maniar & Piccoli (1989), indicating geochemical affinities similar to volcanic arc and collisional granitoids. (d) On the Zr v. (Nb/Zr)N diagram (Thiéblemont & Tégyey, 1994) the granitoids from the study area mostly plot in the continental collision field. Volcanic arc features in some samples are most likely related to the features inherited from previous arc-related protoliths. The migmatitic leucosomes are presented for comparison. A – volcanic and plutonic rocks from subduction zones (island arcs or continental margins) setting; B – rocks emplaced in continent–continent collision zone; C – lavas and plutons from within-plate continental alkaline to transitional provinces and oceanic islands; D – peraluminous rocks of continent–continent collision zones. Nb/Zr ratio normalized to the primordial mantle value (Hoffman, 1988). IAG – island arc granitoids; CAG – continental arc granitoids; CCG – continental collision granitoids; POG – post-orogenic granitoids; RRG – rift-related granitoids; CEUG – continental epeirogenic uplift granitoids; OP – oceanic plagiogranites.

(see Section 1), recent studies based on structural and metamorphic data suggest that continental collision occurred during Oligocene times (Agard *et al.* 2005). Widespread Neogene volcanic activities related to the extensional phase of the Alpine orogeny and U/Pb data from the migmatites provide evidence that the time of collision was Oligocene in the Takab area.

The heat required for partial melting of the crustal rocks may have been supplied from two possible sources. (1) The first is upwelling of mantle plume and advective heating of the crust by deep-seated magma chambers. This can occur in an extensional system with lithospheric thinning (breaking-off of a downward oceanic slab) or may be related to delaminating events in the area (e.g. Ghasemi & Talbot, 2006). Such a model requires crystallization of an unreasonably large volume of mafic magma generated after cessation of subduction and crustal thickening, which is in

disagreement with the scarcity of exposed mafic suites in the study area and so is ruled out on the basis of field and lithological evidence in the Takab area. (2) The heat required for partial melting of the crust has been provided by the continental collision causing crustal thickening (e.g. Agard *et al.* 2005). The second possibility seems to be responsible for generation of the metaluminous granitoids in the Takab area. The ultimate nature of the crustal materials involved and melting conditions are significant factors which caused formation of the collisional sub-alkaline granitoids in the study area.

Melting experiments on basalts demonstrate that H_2O-saturated melting occurs between 750 °C and 800 °C at 5 kbar (Helz, 1976). Rapp (1995) stated that melts formed by dehydration melting of amphibolites are increasingly metaluminous beyond the amphibole-out boundary. Studies by Jung, Hoernes & Mezger
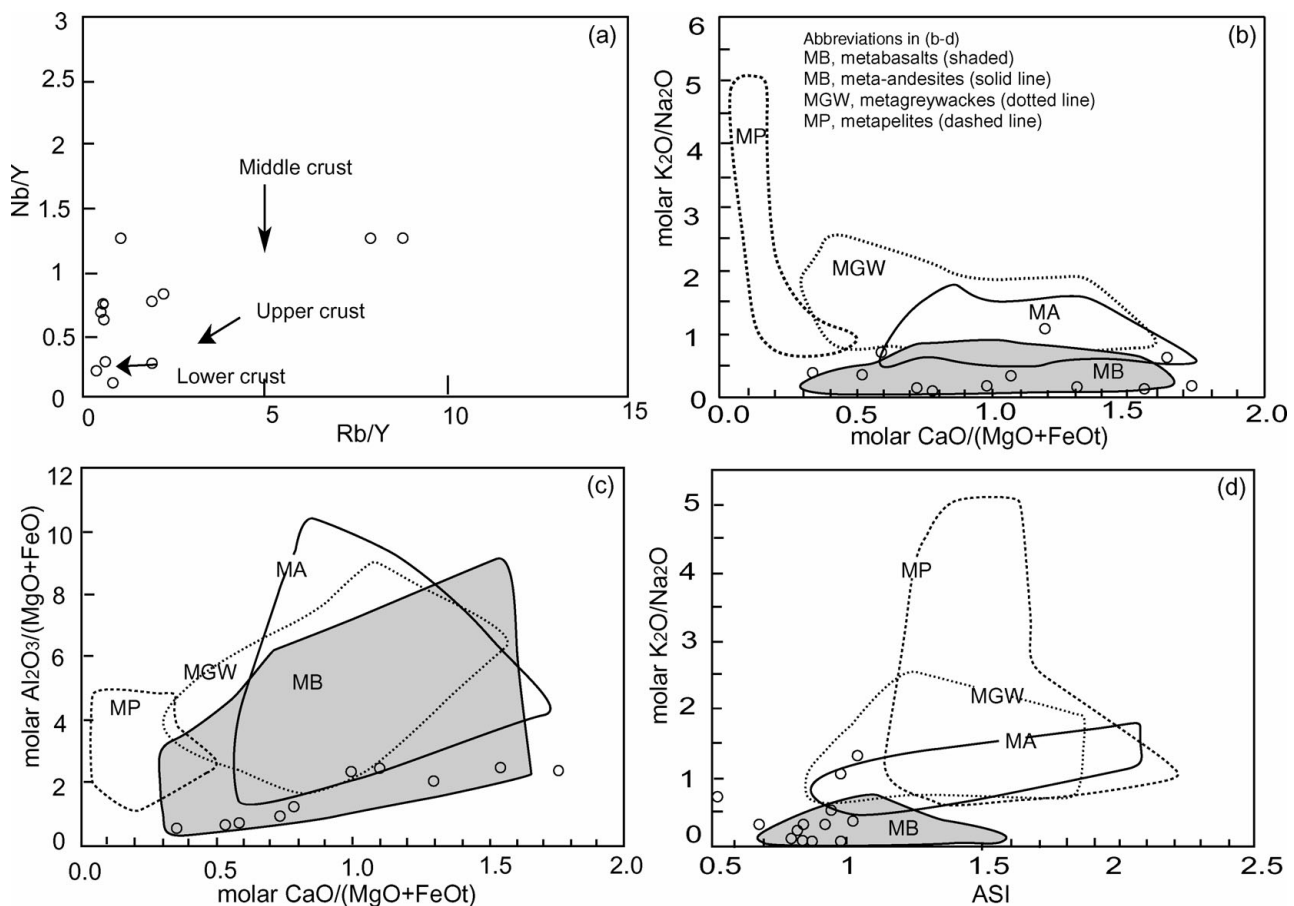
Figure 11. (a) Nb/Y v. Rb/Y diagram for the Takab granitoids. The lower and middle crustal compositions are from Rudnick & Fountain (1995), and the upper crustal compositions are from Taylor & McLennan (1985). (b–d) According to Altherr & Siebel (2002), high concentrations of CaO and low K_2O/Na_2O ratio classify parental rocks as metabasalts. The fields on the diagram are chemical composition of melts from experimental studies of dehydration melting.

(2002), Saleh, Dawood & Abdel-Naby (2002) and Suda (2004) indicate that dehydration melting of amphibolites at temperatures of $900\,°C$ –$1100\,°C$ produces 10–60 % mafic magma ($SiO_2 \sim 50$ wt %) to form tonalite, depending on bulk composition. Based on the experimental data, production of magma with compositions analogous to that of the Takab granitoids takes place under dehydration melting conditions due to hornblende breakdown in amphibolites at a temperature of $900\,°C$ and a pressure range of 5–10 kbar (cf. Wolf & Wyllie, 1991; Wyllie & Wolf, 1993; Rushmer, 1991). Considering field evidence and analogous geochemical characteristics and $P – T$ relations between the granitoids and the migmatitic leucosomes, it seems that the melt which originated from the partial melting of metabasites may have accumulated and the calc-alkaline granitoids of the Takab area have been formed from this melt.

References

AGARD, P., OMRANI, J., JOLIVET, L. & MOUTHEREAU, F. 2005. Convergence history across Zagros (Iran): constraints from collisional and earlier deformation. *International Journal of Earth Sciences* **94**, 401–19.

ALAVI, M. 1994. Tectonics of the Zagros orogenic belt of Iran: new data and interpretations. *Tectonophysics* **229**, 211–38.

ALTHERR, R. & SIEBEL, W. 2002. I-type plutonism in a continental back-arc setting: Miocene granitoids and monzonites from the central Aegean Sea, Greece. *Contributions to Mineralogy and Petrology* **143**, 397–415.

BABAKHANI, A. R. & GHALAMGHASH, J. 1990. *Geological map of Iran, 1:100,000 series sheet Takht-e-Soleiman.* Geological Survey of Iran.

BARKER, F. 1979. *Trondhjemite: definition, environment and hypothesis of origin. In Trondhjemites, dacites and related rocks* (ed. F. Barker), pp. 1–12. Amsterdam: Elsevier.

BECCALUVA, L., MACCIOTTA, G., PICCARDO, G. B. & ZEDA, O. 1989. Clinopyroxene composition of ophiolite basalts

as petrogenetic indicator. *Chemical Geology* **77**, 165–82.

BERBERIAN, M. & KING, G. C. P. 1981. Towards a paleogeography and tectonic evolution of Iran. *Canadian Journal of Earth Sciences* **18**, 210–65.

BERBERIAN, F., MUIR, I. D., PANKHURST, R. J. & BERBERIAN, M. 1982. Late Cretaceous and early Miocene Andean-type plutonic activity in northern Makran and Central Iran. *Journal of the Geological Society, London* **139**, 605–14.

BLUNDY, J. D. & HOLLAND, T. J. B. 1990. Calcic amphibole equilibria and a new amphibole plagioclase geothermometer. *Contributions to Mineralogy and Petrology* **104**, 208–24.

CHAPPELL, B. W. & WHITE, A. J. R. 1974. Two contrasting granite types. *Pacific Geology* **8**, 173–4.

CHRISTOFIDES, G., PERUGINI, D., KORONEOS, A., SOLDATOS, T., POLI, G., ELEFTHERIADIS, G., DEL MORO, A. & NEIVA, A. M. 2007. Interplay between geochemistry and magma dynamics during magma interaction: an example from the Sithonia Plutonic Complex (NE Greece). *Lithos* **95**, 243–66.

COLLINS, W. J., BEAMS, S. D., WHITE, A. J. R. & CHAPPELL, B. W. 1982. Nature and origin of A-type granites with particular reference to southeastern Australia. *Contributions to Mineralogy and Petrology* **80**, 189–200.

DEER, W. A., HOWIE, R. A. & ZUSSMAN, J. 1978. *Rock-forming minerals, 2A, single-chain silicates* (2nd edition). Longman and Wiley.

FROST, B. R., BARNES, G. G., COLLINS, W. J., ARCULUS, R. J., ELLIS, D. J. & FROST, C. D. 2001. A geochemical classification for granitic rocks. *Journal of Petrology* **42**, 2033–48.

GHASEMI, A. & TALBOT, C. J. 2006. A new tectonic scenario for the Sanandaj–Sirjan Zone (Iran). *Journal of Asian Earth Sciences* **26**, 683–93.

GILG, H. A., BONI, M., BALASSONE, G., ALLEN, C. R., BANKS, D. & MOORE, F. 2006. Marble-hosted sulfide ores in the Angouran Zn–(Pb–Ag) deposit, NW Iran: interaction of sedimentary brines with a metamorphic core complex. *Mineralium Deposita* **41**, 1–16.

GUIMARÃES, I. P. & DA SILVA FILHO, A. F. 2000. Evidence of multiple sources involved in the genesis of the neoproterozoic Itapetim granitics complex, NE, Brazil, based on geochemical and isotopic data. *Journal of South American Earth Sciences* **13**, 561–86.

GUIMARÃES, I. P., DA SILVA FILHO, A. F., ALMEIDA, C. N., MELO, E. B., ARAÚJO, J. M. M. & SALES, A. 1998. Sm–Nd isotope geochemistry and U/Pb zircon ages of the Brasiliano granitoids from the Pajeú–Paraíba terrain, Borborema Province, Northeastern Brazil. *South American Symposium Isotope Geology* **2**, 300–1. Córdoba, Anais.

HAGHIPOUR, A. 1974. *Etude geologique de la region de Biabanak-Bafq (Iran Central); petrologie et tectonique du socle Precambrien et de sa couverture.* Theses, Universite Scientifique et Medicale de Grenoble, France, 403 pp. (published thesis).

HAJIALIOGHLI, R., MOAZZEN, M., DROOP, G. T. R., OBERHÄNSLI, R., BOUSQUET, R., JAHANGIRI, A. & ZIEMANN, M. 2007a. Serpentine polymorphs and P–T evolution of meta-peridotites and serpentinites in the Takab area, NW Iran. *Mineralogical Magazine* **71**, 155–74.

HAJIALIOGHLI, R., MOAZZEN, M., JAHANGIRI, A., DROOP, G. T. R., BOUSQUET, R. & OBERHÄNSLI, R. 2007b. Petrogenesis of meta-peridotites in the Takab area, NW Iran. *Goldschmidt Conference Abstracts, Germany*, A370.

HALL, A. 1987. *Igneous Petrology. New York*: John Wiley and Sons, 573 pp.

HAMMARSTROM, J. M. & ZEN, E. A. 1986. Aluminum in hornblende: an empirical igneous geobarometer. *American Mineralogist* **71**, 1297–1313.

HARRIS, N. B. W., PEARCE, J. A. & TINDLE, A. G. 1986. Geochemical characteristics of collision-zone magmatism. In *Collision Tectonics* (eds M. P. Coward & A. C. Ries), pp. 67–81. Geological Society of London, Special Publication no. 19.

HELZ, R. T. 1976. Phase relations of basalts in their melting ranges at $PH_2O=5$ kb. Part II. Melt compositions. *Journal of Petrology* **17**, 139–93.

HOFFMAN, A. W. 1988. Chemical differentiation of the Earth. The relationship between mantle, continental crust and oceanic crust. *Earth and Planetary Science Letters* **90**, 297–314.

HOLLAND, T. & POWELL, R. 1992. Plagioclase feldspars: activity-composition relations based upon Darken's quadratic formalism and Landau theory. *American Mineralogist* **77**, 53–61.

HOLLISTER, L. S., GRISSOM, G. C., PETERS, E. K., STOWELL, H. H. & SISSON, V. B. 1987. Confirmation of the empirical correlation of Al in hornblende with pressure of solidification of calc-alkaline plutons. *American Mineralogist* **72**, 231–9.

IRVINE, T. N. & BARAGAR, W. R. A. 1971. A guide to the chemical classification of the common volcanic rocks. *Canadian Journal of Earth Sciences* **8**, 523–48.

ISHIHARA, S. 1977. The magnetite-series and ilmenite-series granitic rocks. *Mining Geology* **27**, 293–305.

JACKSON, D. D., AKI, K., CORNELL, C. A., DIETERICH, J. H., HENYEY, T. L., MAHDYIAR, M., SCHWARTZ, D. & WARD, S. N. 1995. Seismic hazards in southern California: probable earthquakes, 1994–2024. *Bulletin of the Seismological Society of America* **85**, 379–439.

JOHNSON, M. C. & RUTHERFORD, M. J. 1989. Experimental calibration of the aluminum-in hornblende geobarometer with application to Long Valley caldera (California) volcanic rocks. *Geology* **17**, 837–41.

JUNG, S., HOERNES, S. & MEZGER, K. 2002. Synorogenic melting of mafic lower crust: constraints from geochronology, petrology and Sr, Nd, Pb and O isotope geochemistry of quartz diorites (Damara orogen, Namibia). *Contributions to Mineralogy and Petrology* **143**, 551–66.

KRETZ, R. 1983. Symbols for rock-forming minerals. *American Mineralogist* **68**, 277–9.

KRÖNER, A. & ŞENGÖR, A. M. C. 1990. Archean and Proterozoic ancestry in late Precambrian to early Paleozoic crustal elements of southern Turkey as revealed by single-zircon dating. *Geology* **18**, 1186–90.

KUSHIRO, I. 1960. Si–Al relations in clinopyroxenes from igneous rocks. *American Journal of Science* **258**, 548–54.

LEAKE, B. E., WOOLLEY, A. R., ARPS, C. E. S., BIRCH, W. D., GILBERT, M. C., GRICE, J. D., HAWTHORNE, F. C., KATO, A., KISCH, H. J., KRIVOVICHEV, V. G., LINTHOUT, K., LAIRD, J., MANDARINO, J. A., MARESH, V. W., NICKEL, E. H., ROCK, N. M. S., SCHUMACHER, J. C., SMITH, D. C., STEPHENSON, N. N., UNGARETTI, L., WHITTAKER, E. J. W. & YOUZHI, G. 1997. Nomenclature of amphiboles: report of the subcommittee on amphiboles of the International Mineralogical Association, Commission on New Minerals and Mineral Names. *American Mineralogist* **82**, 1019–37.

LE BAS, M. J. 1962. The role of aluminum in igneous clinopyroxenes with relation to their parentage. *American Journal of Science* **260**, 267–88.

LE MAITRE, R. W. 1976. Some problems of the projection of chemical data into mineralogical classifications. *Contributions to Mineralogy and Petrology* **56**, 181–9.

LETERRIER, J., MAURY, C. R., THONON, P., GIRARD, D. & MARCHAL, M. 1982. Clinopyroxene composition as a method of identification of the magmatic affinities of paleo-volcanic series. *Earth and Planetary Science Letters* **59**, 139–54.

LIÉGEOIS, J. P. & BLACK, R. 1987. Alkaline magmatism subsequent to collision in the Pan-African belt of the Adrar des Iforas (Mali). In *Alkaline Igneous Rocks* (eds J. G. Fitton & B. G. J. Upton), pp. 381–401. Geological Society of London, Special Publication no. 30.

LOOS, S. & REISCHMANN, T. 1999. The evolution of the southern Menderes Massif in SW Turkey as revealed by zircon dating. *Journal of Geological Society, London* **156**, 1021–30.

LOTFI, M. 2001. *Geological map of Iran, 1:100,000 series sheet, Takht-e-Soleiman*. Tehran: Geological Survey of Iran.

MANIAR, P. D. & PICCOLI, P. M. 1989. Tectonic discrimination of granitoids. *Geological Society of America Bulletin* **101**, 635–43.

MAZHARI, S. A., BEA, F., AMINI, S., GHALAMGHASH, J., MOLINA, J. F., MONTERO, P., SCARROW, J. H. & WILLIAMS, I. S. 2009. The Eocene bimodal Piranshahr massif of the Sanandaj–Sirjan Zone, NW Iran: a marker of the end of the collision in the Zagros orogen. *Journal of the Geological Society, London* **166**, 53–69.

MCCARTHY, T. C. & PATIÑO DOUCE, A. E. 1998. Empirical calibration of the silica-Ca-tschermak's-anorthite (SCAn) geobarometer. *Journal of Metamorphic Geology* **16**, 675–86.

MCQUARRIE, N., STOCK, J. M., VERDEL, C. & WERNICKE, B. P. 2003. Cenozoic evolution of Neo-tethys and implications for the causes of plate motions. *Geophysical Research Letters* **30**, 2036.

MIDDLEMOST, E. A. K. 1994. Naming material in the magma/igneous rock system. *Earth Science Reviews* **37**, 215–24.

MOAZZEN, M. & DROOP, G. T. R. 2005. Application of mineral thermometers and barometers to granitoid igneous rocks: the Etive Complex, W Scotland. *Mineralogy and Petrology* **83**, 27–53.

MOAZZEN, M. & HAJIALIOGHLI, R. 2008. Zircon SHRIMP dating of mafic migmatites from NW Iran: reporting the oldest rocks from the Iranian crust. *5th Annual Meeting AOGS, Busan, Korea* SE62.

MOAZZEN, M. & OBERHÄNSLI, R. 2008. Whole rock and relict igneous clinopyroxene geochemistry of ophiolite-related amphibolites from NW Iran – Implications for protolith nature. *Neues Jahrbuch für Mineralogie* **185** (1), 51–62.

MOAZZEN, M., OBERHÄNSLI, R., HAJIALIOGHLI, R., MÖLLER, A., BOUSQUET, R., DROOP, G. T. R. & JAHANGIRI, A. 2009. Peak and post-peak P–T conditions and fluid composition for scapolite–clinopyroxene–garnet calc-silicate rocks from the Takab area, NW Iran. *European Journal of Mineralogy* **21**, 149–62.

MOHAJJEL, M. & FERGUSSON, C. 2000. Dextral transpression in Late Cretaceous continental collision zone, western Iran. *Journal of Structural Geology* **22**, 1125–39.

MOHAJJEL, M., FERGUSSON, C. & SAHANDI, M. R. 2003. Cretaceous–Tertiary convergence and continental collision, Sanandaj-Sirjan zone, western Iran. *Journal of Asian Earth Sciences* **21**, 397–412.

MORIMOTO, N., FABRIES, J., FERGUSON, A. K., GINZBURG, I. V., ROSS, M., SEIFERT, F. A., ZUSSMAN, J., AOKI, K. & GOTTARDI, D. 1988. Nomenclature of pyroxenes. *American Mineralogist* **62**, 53–62.

NAGUDI, B., KOBERT, C. & KURAT, G. 2003. Petrography and geochemistry of the Singo granite, Uganda, and implications for its origin. *Journal of African Earth Sciences* **36**, 73–87.

NANEY, M. T. 1983. Phase equilibria of rock-forming ferromagnesian silicates in granitic systems. *American Journal of Sciences* **283**, 993–1033.

NISBET, E. G. & PEARCE, A. 1977. Clinopyroxene composition in mafic lavas from different tectonic settings. *Contributions to Mineralogy and Petrology* **63**, 149–60.

OPIYO-AKECH, N., TARNEY, J. & HOSHINO, M. 1999. Petrology and geochemistry of granites from Archean terrain north of lake Victoria, Western Kenya. *Journal of African Earth Sciences* **29**, 283–300.

OTTEN, M. T. 1984. The origin of brown hornblende in the Artfjället gabbro and dolerites. *Contributions to Mineralogy and Petrology* **86**, 189–99.

PEARCE, J. A., HARRIS, N. B. W. & TINDLE, A. G. 1984. Trace element discrimination diagrams for the tectonic interpretation of granitic rocks. *Journal of Petrology* **25**, 956–83.

RAMEZANI, J. & TUCKER, R. D. 2003. The Saghand region, central Iran: U–Pb geochronology, petrogenesis and implications for Gondwana tectonics. *American Journal of Sciences* **303**, 622–65.

RAPP, R. P. 1995. Amphibole-out phase boundary in partially melted metabasalt, its control over liquid fraction and composition, and source permeability. *Journal of Geophysical Research* **100**, 15601–10.

RICKWOOD, P. C. 1989. Boundary lines within petrologic diagrams, which use oxides of major and minor element. *Lithos* **22**, 247–63.

ROLLINSON, H. 1993. *Using Geochemical Data: evaluation, presentation, interpretation*. Longman Scientific and Technical, Essex, 352 pp.

RUDNICK, R. L. & FOUNTAIN, D. M. 1995. Nature and composition of the continental crust: a lower crustal perspective. *Reviews of Geophysics* **33**, 267–309.

RUSHMER, T. 1991. Partial melting of two amphibolites: contrasting experimental results under fluid-absent conditions. *Contributions to Mineralogy and Petrology* **107**, 41–59.

SAKI, A. 2010. Proto-Tethyan remnants in northwest Iran: geochemistry of the gneisses and metapelitic rocks. *Gondwana Research* **17** (4), 704–14.

SALEH, G. M., DAWOOD, Y. H. & ABDEL-NABY, H. H. 2002. Petrological and geochemical constraints on the origin of the granitoid suite of the Homert Mikpid area, south Eastern Desert, Egypt. *Journal of Mineralogical and Petrological Sciences* **97**, 47–58.

SAUNDERS, A. D., TARNEY, J. & WEAVER, S. D. 1980. Transverse variations across the Antarctic Peninsula: implications for the genesis of calc-alkaline magmas. *Earth Planetary Science Letters* **46**, 344–60.

ŞENGÖR, A. M. C. 1984. The Cimmeride orogenic system and the tectonics of Eurosia. *Geological Society of America, Special Paper* **195**, 77 pp.

ŞENGÖR, A. M. C., ALTINER, D., CIN, A., USTAOMER, T. & HSU, K. J. 1988. Origin and assembly of the Tethyside orogenic collage at the expense of Gondwana Land. In *Gondwana and Tethys* (eds M. G. Audley-Charles & A.

Hallam), pp. 119–81. Geological of Society of London, Special Publication no. 37.

ŞENGÖR, A. M. C. & NATAL'IN, B. A. 1996. Paleotectonics of Asia: fragments of a synthesis. In *The Tectonic Evolution of Asia* (eds A. Yin & M. Harrison), pp. 486–640. Cambridge University Press.

ŞENGÖR, A. M. C., NATAL'IN, B. A. & BURTMAN, V. S. 1993. Evolution of the Altaid tectonic collage and Palaeozoic crustal growth in Eurasia. *Nature* **364**, 299–307.

ŞENGÖR, A. M. C., ÖZEREN, M. S., KESKIN, M., SAKINÇ, M., ÖZBAKIR, A. D. & KAYAN, I. 2008. Eastern Turkish high plateau as a small Turkic-type orogen: implications for post-collisional crust-forming processes in Turkic-type orogens. *Earth-Science Reviews* **90**, 1–48.

STERN, C. R., HUANG, W. L. & WYLLIE, P. J. 1975. Basalt–andesite–rhyolite–H_2O: crystallization intervals with excess H_2O and H_2O-undersaturated liquidus surface to 35 kilobars, with implications for magma genesis. *Earth and Planetary Science Letters* **28**, 189–96.

STOCKLI, D. F., HASSANZADEH, J., STOCKLI, L. D., AXEN, G., WALKER, J. D. & DEWANE, T. J. 2004. Structural and geochronological evidence for Oligo-Miocene intra-arc low-angle detachment faulting in the Takab-Zanjan area, NW Iran. *Abstracts with Programs, Geological Society of America, Denver Annual Meeting (November 7–10, 2004)* **36**, 319.

STRECKEISEN, A. 1974. Classification and nomenclature of plutonic rocks: recommendations of the IUGS subcommission on the systematics of igneous rocks. *Geologische Rundschau. Internationale Zeitschrift für Geologie, Stuttgart* **63**, 773–85.

SUDA, Y. 2004. Crustal anatexis evolution of granitoid magma in Permian intra-oceanic island arc, the Asago body of the Yakuno ophiolite, Southwest Japan. *Journal of Mineralogical and Petrological Sciences* **99**, 339–56.

SUN, S.-S. & McDONOUGH, W. F. 1989. Chemical and isotopic systematics of oceanic basalts: implications for mantle composition and processes. In *Magmatism in the Ocean Basins* (eds A. D. Saunders & M. J. Norry), pp. 313–45. Geological Society of London, Special Publication no. 42.

TAYLOR, S. R. & McLENNAN, S. M. 1985. *The continental crust: its composition and evolution*. Oxford, England: Blackwell Scientific Publications, 312 pp.

THIÉBLEMONT, D. & TÉGYEY, M. 1994. Une discrimination géochimique des roches différenciés témoin de la diversité d'origine et de situation tectonique des magmas calco-alcalins. *Académie des Sciences, Paris* **319**, 87–94.

VERDEL, C., WERNICKE, B. P., RAMEZANI, J., HASSANZADEH, J., RENNE, P. R. & SPELL, T. L. 2007. Geology and thermochronology of Tertiary Cordilleran-style metamorphic core complexes in the Saghand region of central Iran. *Geological Society of America Bulletin* **119**, 961–77.

VERHOOGEN, J. 1962. Distribution of titanium between silicates and oxides in igneous rocks. *American Journal of Sciences* **260**, 211–20.

VYHNAL, C. R., McSWEEN, H. Y. & SPEER, J. A. 1991. Hornblende chemistry in southern Appalachian granitoids: implications for aluminum in hornblende thermobarometry and magmatic epidote stability. *American Mineralogist* **6**, 176–88.

WHALEN, J. B. & CHAPPELL, B. W. 1988. Opaque mineralogy and mafic mineral chemistry of I-and S-type granites of the Lachlan fold belt, southeast Australia. *American Mineralogist* **73**, 281–96.

WOLF, M. B. & WYLLIE, P. J. 1991. Dehydration-melting of solid amphibolite at 10 kbar: textural development, liquid interconnectivity and applications to the segregation of magmas. *Mineralogy and Petrology* **44**, 151–79.

WOOD, B. J. 1979. Activity-composition relationships in $Ca(Mg, Fe)Si_2O_6$–$CaAl_2SiO_6$ clinopyroxene solid solutions. *American Journal of Sciences* **279**, 854–75.

WYLLIE, P. J. & WOLF, M. B. 1993. Amphibolite-dehydration melting: sorting out the solidus. In *Magmatic processes and plate tectonics* (eds H. M. Pritchard, T. Alabaster, N. B. W. Harris & C. R. Neary), pp. 405–16. Geological Society of London, Special Publication no. 76.

ZEN, E. & HAMMARSTROM, J. M. 1984. Magmatic epidote and its petrologic significance. *Geology* **12**, 515–18.

ZEN, E. & HAMMARSTROM, J. M. 1988. Plumbing the depths of plutons by magmatic epidote–hornblende association: A cautionary review and example from the Round Valley pluton, western Idaho. *Programs, Geological Society of America* **20**, 475–6.